Colloids and Surfaces A: Physicochem. Eng. Aspects 509 (2016) 521–538

Contents lists available at ScienceDirect

Colloids and Surfaces A: Physicochemical and Engineering Aspects

journal homepage: www.elsevier.com/locate/colsurfa

Limited coalescence and Ostwald ripening in emulsions stabilized by hydrophobin HFBII and milk proteins

Lydia M. Dimitrova[a], Mariana P. Boneva[a], Krassimir D. Danov[a], Peter A. Kralchevsky[a,*], Elka S. Basheva[a], Krastanka G. Marinova[a], Jordan T. Petkov[b,1], Simeon D. Stoyanov[c,d,e]

[a] Department of Chemical and Pharmaceutical Engineering, Faculty of Chemistry and Pharmacy, Sofia University, 1164 Sofia, Bulgaria
[b] Unilever Research & Development, Port Sunlight, Wirral, Merseyside CH63 3JW, UK
[c] Unilever Research & Development Vlaardingen, 3133AT Vlaardingen, The Netherlands
[d] Laboratory of Physical Chemistry and Colloid Science, Wageningen University, 6703 HB Wageningen, The Netherlands
[e] Department of Mechanical Engineering, University College London, WC1E 7JE, UK

HIGHLIGHTS

- Solidification threshold of HFBII layers at o/w interfaces is determined and interpreted.
- The thinning of o/w/o emulsion films with HFBII ends with the formation of S-bilayer.
- The law of limited coalescence in emulsions with HFBII is quantitatively interpreted.
- Emulsions with HFBII are stable for at least 50 days at rest but unstable upon stirring.
- The dense HFBII adsorption layers encapsulate volatile oils and block Ostwald ripening.

GRAPHICAL ABSTRACT

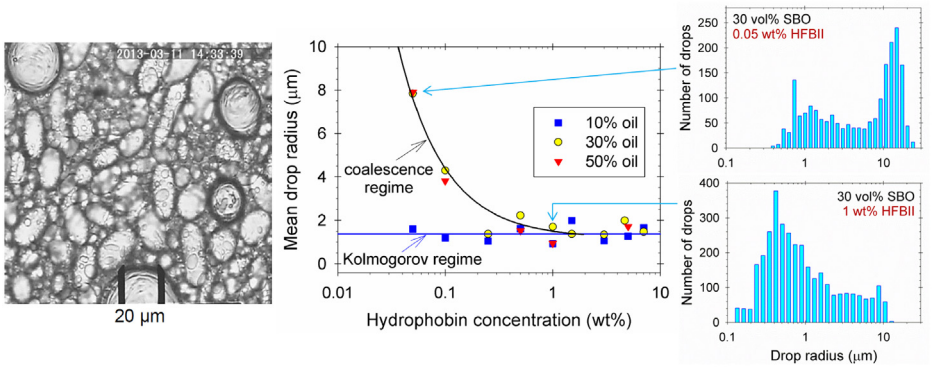

ARTICLE INFO

Article history:
Received 10 August 2016
Received in revised form
15 September 2016
Accepted 16 September 2016
Available online 16 September 2016

Keywords:
HFBII hydrophobin
Emulsification
Emulsion stability
Ostwald ripening
Drop size distribution

ABSTRACT

Hydrophobins are proteins isolated from filamentous fungi, which are excellent foam stabilizers, unlike most of the proteins. In the present study, we demonstrate that hydrophobin HFBII can also serve as excellent emulsion stabilizer. The HFBII adsorption layers at the oil/water interface solidify similarly to those at the air/water interface. The thinning of aqueous films sandwiched between two oil phases ends with the formation of a 6 nm thick protein bilayer, just as in the case of foam films, which results in strong adhesive interactions between the emulsion drops. The drop-size distribution in hydrophobin stabilized oil-in-water emulsions is investigated at various protein concentrations and oil volume fractions. The data analysis indicates that the emulsification occurs in the Kolmogorov regime or in the regime of limited coalescence, depending on the experimental conditions. The emulsions with HFBII are very stable – no changes in the drop-size distributions are observed after storage for 50 days. However, these emulsions are unstable upon stirring, when they are subjected to the action of shear stresses. This instability can be removed by covering the drops with a second adsorption layer from a conventional protein, like β-lactoglobulin. The HFBII surface layer is able to suppress

* Corresponding author.
E-mail address: pk@lcpe.uni-sofia.bg (P.A. Kralchevsky).
[1] Present address: Lonza, Hexagon Tower, Crumpsall Vale, Blackley, Manchester, M9 8GQ, UK.

http://dx.doi.org/10.1016/j.colsurfa.2016.09.066

the Ostwald ripening in the case when the disperse phase is oil that exhibits a pronounced solubility in water. Hence, the hydrophobin can be used to stabilize microcapsules of fragrances, flavors, colors or preservatives due to its dense adsorption layers that block the transfer of oil molecules.

1. Introduction

Hydrophobins are a class of relatively small proteins (65–100 amino acid residues), which are exclusively produced by filamentous fungi, including some edible mushrooms [1–3]. These proteins possess several remarkable properties. First, the hydrophobin molecules are strongly amphiphilic, like Janus particles, with hydrophobic and hydrophilic patches expressed on their surfaces [1,4]. Second, at air/water and oil/water interfaces they self-assemble into dense adsorption layers (membranes) of high surface dilatational and shear elasticity, which exceeds the elasticity of all other investigated proteins [5–9]. The presence of shear elasticity indicates that the hydrophobin adsorption layers at the air/water interface are not fluid – they solidify soon after their formation [7,10,11]. Third, the hydrophobins are "sticky" proteins [11] – they have been utilized for immobilizing functional molecules at surfaces [12], and for surface modification by appropriate coatings [13].

In the present study, the class II hydrophobin HFBII was used. The structure of HFBII determined from crystallized samples shows that it is a single-domain protein with dimensions of $24 \times 27 \times 30$ Å [14]. In aqueous solutions, it forms aggregates, which are predominantly tetramers at mg/mL concentrations [15–18]. Because of the adhesive interactions between the HFBII molecules in water, these aggregates can irreversibly grow with time and can reach micrometer sizes [19–21]. The formed large aggregates can be destroyed by ultrasound treatment (sonication). The adsorption of HFBII at air/water and liquid/solid interfaces has been also studied [22–24]. Not only the hydrophobic, but also the hydrophilic parts of HFBII molecules attract each other in aqueous medium, which is evidenced by the strong adhesion between the surfaces of foam films (contact angle >50°) and the spontaneous formation of self-assembled protein bilayers (S-bilayers) of thickness 6 nm [20,25].

Unlike most of the proteins, the hydrophobins are excellent *foam stabilizers* [5,19,26–28]. The Ostwald ripening that is due to diffusion transfer of gas from the smaller to the bigger bubbles [29], can be blocked by the dense and mechanically strong HFBII membranes, which prevent also the bubble coalescence. Detailed literature review and experimental results on hydrophobin stabilized foams can be found in our previous article [30].

The properties of hydrophobins as *emulsifiers* are much less studied in comparison with their properties as foaming agents. Stabilization of emulsion drops (of olive oil in water) by SC3 hydrophobin was first reported by Wösten et al. [31] and it was suggested that oil vesicles covered with hydrophobin membrane could find applications in drug delivery [32,33]. Lumsdon et al. [34] presented data for the stabilization of polyunsaturated fatty acid oil-in-water emulsions by HFBII. Ascolin et al. [35] compared different hydrophobins as emulsifiers and reported that oil-in-water emulsions prepared with HFBI and SC3 were more stable than those with HFBII. Reger et al. [36] investigated emulsions stabilized by two types biotechnically produced water-soluble recombinant hydrophobins and studied the rheology of these emulsions. Further, these authors demonstrated that the combined action of hydrophobins and clay particles produce synergistic effect on emulsification and emulsion stability [37–40]. Cox et al. [41,42] established that hydrophobin HFBII can be used as stabilizer of aerated emulsions for the food industry. Khalesi et al. [43] demonstrated that HFBII membranes can be used for encapsulation and retention of the volatile oil ocimene in the water phase. It was established that the HFBII molecule is stable at the oil/water interface, where it undergoes minimal conformational changes [44]. The surface shear rheology of hydrophobin adsorption layers at oil/water interfaces was also investigated [45].

It should be noted that none of the above studies presents systematic data for the effect of protein concentration and oil volume fraction on the oil-drop distribution and longevity of hydrophobin stabilized emulsion. The present article is the first systematic study of the properties of HFBII as emulsifier. First, we investigate whether the hydrophobin adsorption layers solidify on the oil/water interfaces, as this is observed at the air/water interface. The threshold interfacial tension at solidification is determined (Section 4). Next, in experiments with o/w/o emulsion films we study the interaction of two HFBII adsorption layers across the aqueous phase. One of our goals is to verify whether S-bilayers can be formed also with emulsion films (Section 5). Further, by optical observations we investigate the shape and size distribution of the drops in HFBII stabilized emulsions; calculate the mean drop radii, R_{10} and R_{32}, and study their dependence on the protein concentration, oil volume fraction and emulsion storage time, up to 50 days (Section 6). It turns out, that the emulsions with HFBII are very stable at rest, but they can be easily destabilized upon stirring. This is due to the fact that the solidified structure of adherent oil drops covered by hydrophobin adsorption layers is destroyed by the shear stresses. It is demonstrated that if the emulsion drops are wrapped with a second layer of conventional protein (like β-lactoglobulin), the emulsions become stable upon stirring and centrifugation (Section 7). Finally, we investigated whether the dense hydrophobin adsorption layers can block the Ostwald ripening, which is one of the main destabilizing factors in emulsions where the disperse phase is oil that exhibits pronounced water solubility [46]. Two such oils, limonene and xylene, have been investigated and the stabilizing performance of HFBII was compared with that of other emulsifiers (Section 8).

2. Materials and methods

2.1. Materials

The proteins used in our experiments were as follows:

(1) Hydrophobin HFBII; 70 amino acids; molecular weight M_w = 7.2 kDa; 4 disulfide bonds. The used HFBII sample, provided as a gift by Unilever R&D, was produced via fermentation using *Trichoderma reesei* [20].
(2) β-lactoglobulin (BLG) from bovine milk; 162 amino acids; M_w = 18.3 kDa; 2 disulfide bonds. The used sample was product of Sigma (≥90%, Cat. No. L0130).
(3) The skim milk powder (SMP), received from Unilever, contains 35 wt% protein, mostly caseins and whey proteins; the rest is lactose and some minerals.

As water-soluble surfactant, we used the nonionic surfactant Tween 20 (polyoxyethylene 20-sorbitan monolaurate, $C_{58}H_{114}O_{26}$), molecular weight 1228 g/mol, Sigma, cat. No. 93773. The critical micelle concentration (CMC) of Tween 20 is about 50 μM [47]. In some experiments, sodium dodecyl sulfate (SDS, molecular weight 288.37 g/mol, product of Acros) was also used.

The used soybean oil (SBO) was a food grade commercial product from a local producer, which was purified by passing through a column filled with adsorbents Florisil and Silica gel 60. Three consecutive passages were applied in order to obtain oil that was free of polar contaminants, as indicated by the constancy of the interfacial tension, which was 30.5 ± 0.5 mN/m, which is close to the literature value of 31 mN/m [48]. The viscosity of SBO is 54.3 mPa s and its density is 0.920 g/cm^3. Because SBO is insoluble in water, the evolution of drop-size distribution in SBO-in-water emulsions could be due to drop coalescence, rather than to Ostwald ripening. To study whether the used emulsifiers could prevent the Ostwald ripening, we investigated also emulsions prepared from two kinds of oils that exhibit pronounced water solubility:

Limonene (4-isoprenyl-1-methylcyclohexene) was used as it was received from Sigma (cat. No. W524905). The viscosity of limonene is 10 mPa s, its density is 0.841 g/cm^3; molecular weight 136.24 g/mol, and its solubility in water is 13.8 mg/L at 25 °C [49,50].

Another oil of known solubility in water was *xylene* (dimethylbenzene, C_8H_{10}) product of Teokom, cat. No. 202-4222-2 (mixture of *ortho*-, *meta*- and *para*-xylene). Its viscosity is 0.61 mPa s; density 0.864 g/cm^3; molecular weight 106.16 g/mol and its solubility in water is in the range 161–178 mg/L at 25 °C [50].

For the preparation of all solutions, deionized water of specific resistivity 18.2 MΩ cm (Mili-Q Organex system, Millipore) was used. The water phase in all emulsions contained 0.1 g/L of the antibacterial agent NaN_3 (product of Merck, molecular weight 65.01 g/mol, cat. No. 247-852-1).

2.2. Methods

Interfacial tension measurements were carried out by forming and observing small drops by means of the *drop shape analysis* system DSA100 M (Krüss GmbH, Germany); see Fig. A.1 in Appendix A. Two different regimes were used to determine the interfacial tension. In the first (standard) regime, called for brevity DSA, the pendant drop method was used, which is based on fits of the instantaneous drop profiles by solving the Laplace differential equation of capillarity. In the second regime, called *capillary pressure tensiometry* (CPT), a small (spherical) drop is formed at the tip of a capillary and then the interfacial tension, σ, is determined from the simple version of Laplace equation, $\sigma = RP_c/2$, where R and P_c are, respectively, the experimental drop radius and capillary pressure. The latter was measured by a pressure transducer; see Ref. [51] for details.

The Scheludko–Exerowa (SE) cell [52] was used in the experiments with individual free *emulsion films*. Thin films were formed by sucking out the aqueous phase from a biconcave meniscus held in a glass capillary of inner radius 1.5 mm, immersed in the oil. The thickness of the film, h, can be measured by means of an interferometric method [52,53]. For this purpose, the light reflected from the film is supplied to a photomultiplier and computer, and the film thickness is recorded in the course of the experiment. The observations were carried out by microscope in reflected monochromatic light of wavelength $\lambda = 546$ nm through the optically clear cover of the cell. The studied thin films look darker if their thickness is smaller; for details see Ref. [53].

The *emulsification* was performed by rotor-stator homogenizer Ultra Turrax T25 digital (IKA-Germany) operating between 3000 and 25000 rpm with dispersing tool S25N−10G. The emulsions were prepared in 100 mL beakers. The total volume of the liquid (water and oil phases) was 40 mL. First, the glass vessel filled with the liquid phases was sonicated for 20 s in a water bath to disperse the protein aggregates. (The sonication power was sufficiently low to avoid any sonochemical effects.) Next, we prepared an emulsion premix by Ultra Turrax operating at 12000 rpm for 3 min, and finally, the premix was subjected to stirring at 24,000 rpm for 5 min.

2.3. Microscopic observations of the emulsions

The drop-size distributions were obtained for freshly prepared emulsions and for emulsions that have been stored for a given period of time. The used procedure for obtaining the drop-size distribution involves dilution of the emulsion and measuring the sizes of the separate drops. In our experiments, to prevent the drop coalescence, a portion of the respective original emulsion was diluted with 5 mM SDS solution and gently shaken to disperse the droplets. At that, droplets of ellipsoidal shape covered by solidified HFBII adsorption layers acquired spherical shape in the SDS solution. Moreover, flocs of drops were split to separate spherical drops. Next, samples for optical observations were taken. A small portion of the diluted emulsion was loaded in a capillary of rectangular cross-section (Vitro Tubes, 0.10 × 1.00 mm, cat. No 5010-050) and observed by Axioplan microscope, equipped with an objective Epiplan, 50×, and connected to a CCD camera and digital video recorder. For each sample, the diameters of at least 1000 drops were measured (one by one, semi-automatically) by using image-analysis. To ensure correct statistics, we processed video frames corresponding to different positions of the focal plane inside the emulsion.

The emulsion preparation and microscopic observations were carried out at room temperature, 25 °C. The emulsions were stored at different temperatures (specified further in the text) to investigate their stability with respect to drop coalescence and Ostwald ripening.

3. Drop-size distributions and emulsification regimes

3.1. Processing of data for the drop-size distribution

The semi-automatic image analysis yields a set of data for the drop radii, $\{R_i\}_{i=1}^{N}$, where R_i is the radius of the i-th drop, and N is the total number of counted drops in the studied sample. The arithmetic mean radius, R_{10}, and the volume-to-surface mean radius, R_{32}, have been calculated using the standard formulas:

$$R_{10} = \frac{1}{N}\sum_{i=1}^{N} R_i \text{ and } R_{32} = \left(\sum_{i=1}^{N} R_i^3\right) / \left(\sum_{i=1}^{N} R_i^2\right) \quad (1)$$

The values of R_{10} and R_{32} calculated from Eq. (1) and the respective histograms are given below to characterize the experimental drop-size distributions.

For statistical data analysis, the experimental *cumulative function* was calculated. First, the radii of a set of N emulsion droplets, measured as explained above, are ordered in an ascending series, $R_1, R_2, \ldots, R_K$, where K is the total number of different drop radii. Each drop radius, R_k, appears n_k times in the original data set, $k = 1, 2, \ldots, K$. Thus, the total number of drops is

$$N = \sum_{k=1}^{K} n_k \quad (2)$$

By definition, the cumulative function, $f(R_k)$, is equal to the number of drops of radii $R \le R_k$. The function $f(R_k)$ is normalized by the total drop number N [54]:

$$f(R_k) = \frac{1}{N}\sum_{j=1}^{k} n_j \tag{3}$$

By means of Eq. (3), one can calculate $f(R_k)$ for each experimentally measured R_k ($k = 1, 2, \ldots, K$).

In the case of *lognormal distribution*, the probability function, $p(R)$, reads:

$$p(R) = \frac{1}{\sqrt{2\pi}}\frac{1}{\ln\sigma}\exp\left[-\frac{\ln^2(R/R_d)}{2\ln^2\sigma}\right] \tag{4}$$

where R_d is the mean drop radius and σ is the dimensionless dispersion ($\sigma > 1$). The peak of $p(R)$ defined by Eq. (4) is symmetric in logarithmic scale. The radii of 50% of the drops belong to the interval $R_d/\sigma \le R \le R_d\sigma$, which characterizes the polydispersity of the respective drop-size distribution. The cumulative function, which corresponds to the lognormal distribution, is:

$$f(R) \equiv \int_{-\infty}^{\ln R} p(\xi)\mathrm{d}(\ln\xi) = \frac{1}{2}\left\{1 + \mathrm{erf}\left[\frac{\ln(R/R_d)}{\sqrt{2}\ln\sigma}\right]\right\} \tag{5}$$

where erf(x) is the error function [55] and ξ is an integration variable. The experimental cumulative function $f(R_k)$ given by Eq. (3) was fitted with the theoretical dependence $f(R)$ given by Eq. (5). The values of R_d and σ were determined as adjustable parameters.

In some cases, the experimental drop-size distribution is closer to a *bimodal lognormal distribution*. The expression for the probability function, $p(R)$, for this distribution is a superposition of those for two different unimodal lognormal distributions with probabilities β_1 and $\beta_2 = 1 - \beta_1$, mean radii R_{d1} and R_{d2}, and dimensionless dispersions σ_1 and σ_2 [54]:

$$p(R) = \frac{1}{\sqrt{2\pi}}\sum_{i=1}^{2}\frac{\beta_i}{\ln\sigma_i}\exp\left[-\frac{\ln^2(R/R_{di})}{2\ln^2\sigma_i}\right] \tag{6}$$

The cumulative function, $f(R)$, corresponding to the bimodal lognormal distribution is [54]:

$$f(R) \equiv \int_{-\infty}^{\ln R} p(\xi)\mathrm{d}(\ln\xi) = \sum_{i=1}^{2}\frac{\beta_i}{2}\left\{1 + \mathrm{erf}\left[\frac{\ln(R/R_{di})}{\sqrt{2}\ln\sigma_i}\right]\right\} \tag{7}$$

In the cases with bimodal distribution, the experimental cumulative function $f(R_k)$ given by Eq. (3) was fitted by means of the theoretical dependence $f(R)$ given by Eq. (7). The values of β_1, R_{d1}, R_{d2}, σ_1, and σ_2 were determined as adjustable parameters.

3.2. Emulsification regimes

Two different regimes of emulsification could be experimentally observed, limited coalescence [56–59] and Kolmogorov regime [60–65]. In the *limited coalescence* regime, which takes place at lower protein concentrations and/or higher oil volume fractions, the protein adsorption layers on the drop surfaces are not dense enough to prevent the drop coalescence. Each act of coalescence of two drops leads to transfer of the adsorbed molecules on the surface of the produced bigger drop, which has smaller surface area than the area of the two initial drops. This leads to the formation of denser adsorption layers that eventually block the further drop coalescence. The hydrophobin is a strongly surface active molecule that forms aggregates in the aqueous phase. If the stirring during the emulsification is sufficiently long and intensive, we may assume that practically the *whole* amount of HFBII has been adsorbed at the surfaces of the formed emulsion drops, where it forms *dense* adsorption layers that consist of adsorbed aggregates, the smallest "aggregates" being the protein molecules. In such a case, the volume-to-surface mean drop radius R_{32} can be expressed in the form [66]:

$$R_{32} = \frac{4\rho_{HFBII}}{\rho_w}\frac{\Phi_{oil}}{1-\Phi_{oil}}\frac{a_{32}}{C_{HFBII}} \tag{8}$$

where Φ_{oil} is the volume fraction of oil in the emulsion; ρ_{HFBII} and ρ_w are the mass densities of HFBII and water; C_{HFBII} is the weight fraction of HFBII in the aqueous phase; the area fraction of the adsorbed protein has been assumed equal to 1 (for a dense HFBII adsorption layer) and a_{32} is the volume-to-surface mean radius of the HFBII aggregates adsorbed on the drop surfaces:

$$a_{32} = \left(\sum_{i=1}^{N} a_i^3\right) / \left(\sum_{i=1}^{N} a_i^2\right) \tag{9}$$

The derivation of Eq. (8) in the case of monodisperse aggregates can be found in Refs. [58,67,68], and in its general form for polydisperse aggregates – in Ref. [30]. Here, we will use the following parameter values: $\rho_w \approx 1\,\mathrm{g/cm^3}$ for water and $\rho_{HFBII} = 1.5\,\mathrm{g/cm^3}$ for hydrophobin. The last value was estimated from the empirical dependence of the protein mass density on the protein molecular mass [69].

As an illustration for the application of Eq. (8), let is calculate what protein concentration in the solution, C_{HFBII}, would be necessary to cover all oil droplets in an emulsion of mean drop radius $R_{32} = 1\,\mu\mathrm{m}$ with a monolayer of hydrophobin, if all the emulsifier is adsorbed and if the oil volume fraction is $\Phi_{oil} = 0.3$. By substituting the given parameter values in Eq. (8), we calculate $C_{HFBII} = 0.17$ wt%.

At higher protein concentrations and/or lower oil volume fractions the emulsification occurs in the *Kolmogorov regime*. In this regime, the drop size distribution is determined by the input of energy by the homogenizer. In other words, all formed drops are stable. As established in the studies by Kolmogorov [60] and Hinze [61], the mean diameter of the drops is determined by the interaction of the emulsion drops with the turbulent eddies created by the homogenizer. It is presumed that the surfactant concentration is high enough, so that the formed drops do not coalesce; see also Refs. [62–65]. Two different regimes of drop breakage by the eddies have been identified: (i) In turbulent-*inertial* regime, the eddies are comparable by size or smaller than the drops and could break them upon collision. (ii) In turbulent-*viscous* regime, the eddies are bigger than the drops and act like a mill. As a rule, the drops produced in the viscous regime are smaller than those produced in the inertial regime. The Kolmogorov expressions for the mean diameter, d_K, of the drops produced in the two regimes are [60–65]:

$$d_K \approx \varepsilon^{-2/5}\sigma^{3/5}\rho_c^{-1/5}(\text{inertial regime}) \tag{10}$$

$$d_K \approx \varepsilon^{-1/2}\sigma\eta_c^{-1/2}(\text{viscous regime}) \tag{11}$$

where ε is the input mechanical energy per unit time and per unit volume; σ is the oil/water interfacial tension; η_c and ρ_c are, respectively, the viscosity and mass density of the continuous phase (in our case – water). Note that d_K in Eqs. (10) and (11) depends neither on protein concentration, C_{HFBII}, nor on the oil volume fraction, Φ_{oil}, unlike the case of limited coalescence described by Eq. (8).

4. HFBII adsorption layers at the oil/water interface

4.1. Interfacial tension

First, we verified whether HFBII hydrophobin is soluble in the oil phase (SBO). For that purpose, a certain amount of HFBII was placed in a glass jar; soybean oil was added and stirring with mixer was applied. As a result, a turbid suspension was produced with

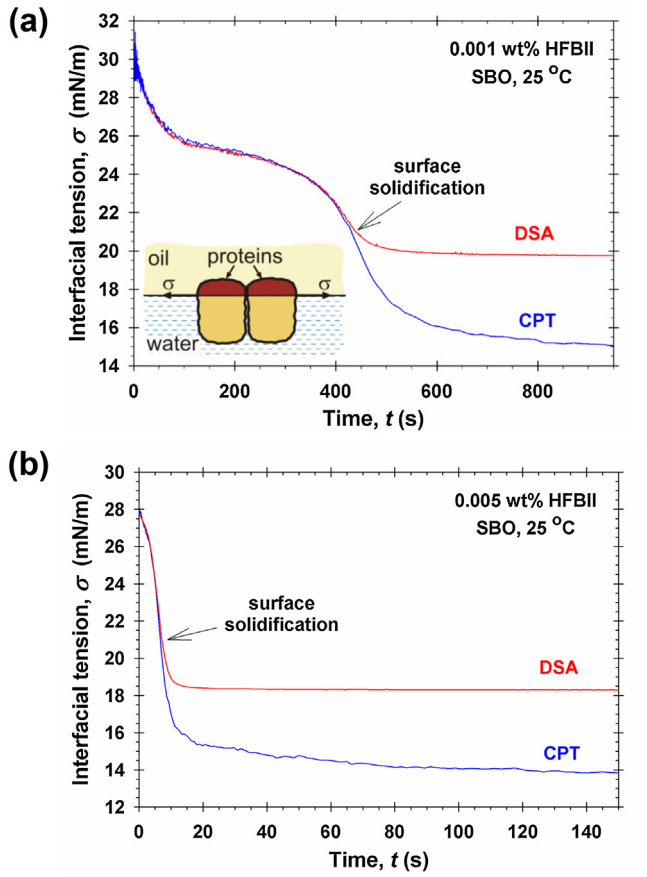

Fig. 1. Time dependencies of the interfacial tension, σ, determined by the pendant drop method + DSA, and of the local value of the interfacial tension at the drop apex measured by capillary pressure tensiometry (CPT) at two HFBII concentrations in the water phase: (a) 0.001 wt% and (b) 0.005 wt%. The inset illustrates the derivation of Eq. (12).

large pieces of solid HFBII. The interfacial tension, σ, of the oil with HFBII against pure water was measured by DSA with pendant aqueous drops. The measured σ values were the same as for SBO/water without HFBII for more than 35 min. Thus, we can conclude that HFBII is not soluble in soybean oil in molecular form or in the form of oligomers, as it is in water. Analogous result was obtained with hexadecane (instead of SBO).

Experimentally, the solidification (if any) of the protein adsorption layer can be detected by comparing the values of σ obtained by the CPT and DSA methods. CPT yields the interfacial tension σ of a small spherical drop, which is presumably uniform and isotropic because of the uniform curvature. More precisely, CPT yields the value of σ in the drop apex, where the assumption for isotropy is always satisfied. The DSA method works with bigger drops, deformed by gravity, and gives the correct value of σ for fluid interfaces only. In the case of solidified adsorption layer, DSA gives incorrect σ [70]. This is because the assumption that σ is isotropic even for deformed drops fails in the case of solidified adsorption layer, for which the interfacial tension is a non-isotropic (tensorial) quantity [10,11]. In such a case, the surface tension has different values along the "parallels" and "meridians" on the drop surface, which could be determined in each point by the method of capillary meniscus dynamometry [11,70].

Fig. 1 shows data for the relaxation kinetics of σ determined by CPT and DSA at two HFBII concentrations in the aqueous phase, 0.001 and 0.005 wt%. As expected, at the higher protein concentration the relaxation of σ is much faster. Comparing Fig. 1a and b, one sees that at both HFBII concentrations the values of σ obtained

Table 1
Values of the interfacial tension, σ^*, and surface pressure, π_s, at the phase transition in HFBII adsorption layers (Fig. 1).

Interface	σ^* (mN/m)	π_s (mN/m)
air-water [7]	50	22
SBO-water	21	10
hexadecane-water	21	33

by the two methods become different for $\sigma < 21$ mN/m. Hence, $\sigma \approx 21$ mN/m can be considered as solidification threshold of the protein adsorption layer. At that, for $\sigma < 21$ mN/m CPT gives the correct value of surface tension at the drop apex, whereas the greater value given by DSA is incorrect insofar as DSA is inapplicable to solidified interfaces [70].

The DSA method gives not only the interfacial tension, σ, but also the *error of the fit* of the drop profile by means of the Laplace differential equation of capillarity. The DSA data show that for $\sigma \leq 21$ mN/m the fit error exhibits a steep increase indicating that the experimental profile does not obey the Laplace equation; see Fig. A.2 in Appendix A and Ref. [7]. Thus, the error of the Laplace fit can serve as a second indicator for the solidification of the HFBII adsorption layer on the SBO/water interface, which confirms the result in Fig. 1.

Analogous experiments with hexadecane show that the surface phase transition takes place at the *same* value of σ as for SBO (Table 1). Note that the values of σ for the pure oil/water interface are rather different for SBO and hexadecane: 31 vs 52 mN/m. The fact that for these two different oil/water interfaces the solidification of the protein adsorption layer happens at the same threshold interfacial tension, $\sigma^* \approx 21$ mN/m, might not be an occasional coincidence. Why is the solidification determined by the surface tension σ, rather than by the surface pressure π_s? An idea for possible explanation is proposed below.

Let us consider two protein (e.g. HFBII) molecules at the oil/water interface, which are pressed against each other; see the inset of Fig. 1a. The two molecules will adhere if the net attraction force between them, F_{attr}, is greater than the surface tension force, F_σ, which tends to separate the protein molecules: $F_{attr} > F_\sigma = \sigma L$; here L is the length of the molecule in the zone of contact. In other words, the two molecules will adhere if σ is smaller than the following threshold value:

$$\sigma < \frac{F_{attr}}{L} \equiv \sigma* \tag{12}$$

In our case, the threshold value is $\sigma^* = 21$ mN/m; the molecular length is $L \approx 3$ nm. Then, from Eq. (12) we could estimate that the net attraction force between the two adsorbed HFBII molecules is $F_{attr} = 63$ pN for the oil/water interface.

The greater value of the threshold tension, $\sigma^* \approx 50$ mN/m, for hydrophobin at the air/water interface (Table 1) could be explained with a greater F_{attr} due to stronger attraction between the hydrophobic caps of the HFBII molecules across air (in comparison with the attraction in oily environment); i.e. $F_{attr} \approx 150$ pN for the air/water interface. In this way, from the threshold interfacial tension for solidification of the protein adsorption layer, σ^*, one could estimate the net attraction between two protein molecules at contact, F_{attr}.

4.2. Irreversibility of hydrophobin adsorption

Here, we check whether the adsorption of HFBII at the oil/water interface is reversible or irreversible. For this goal, we used the DSA method. A buoyant SBO drop was formed on the tip of a J-shaped needle dipped in aqueous solution of HFBII. The results of a typical experiment are shown in Fig. 2. Initially, the interfacial tension σ fast decreases owing to the HFBII adsorption at the oil/water

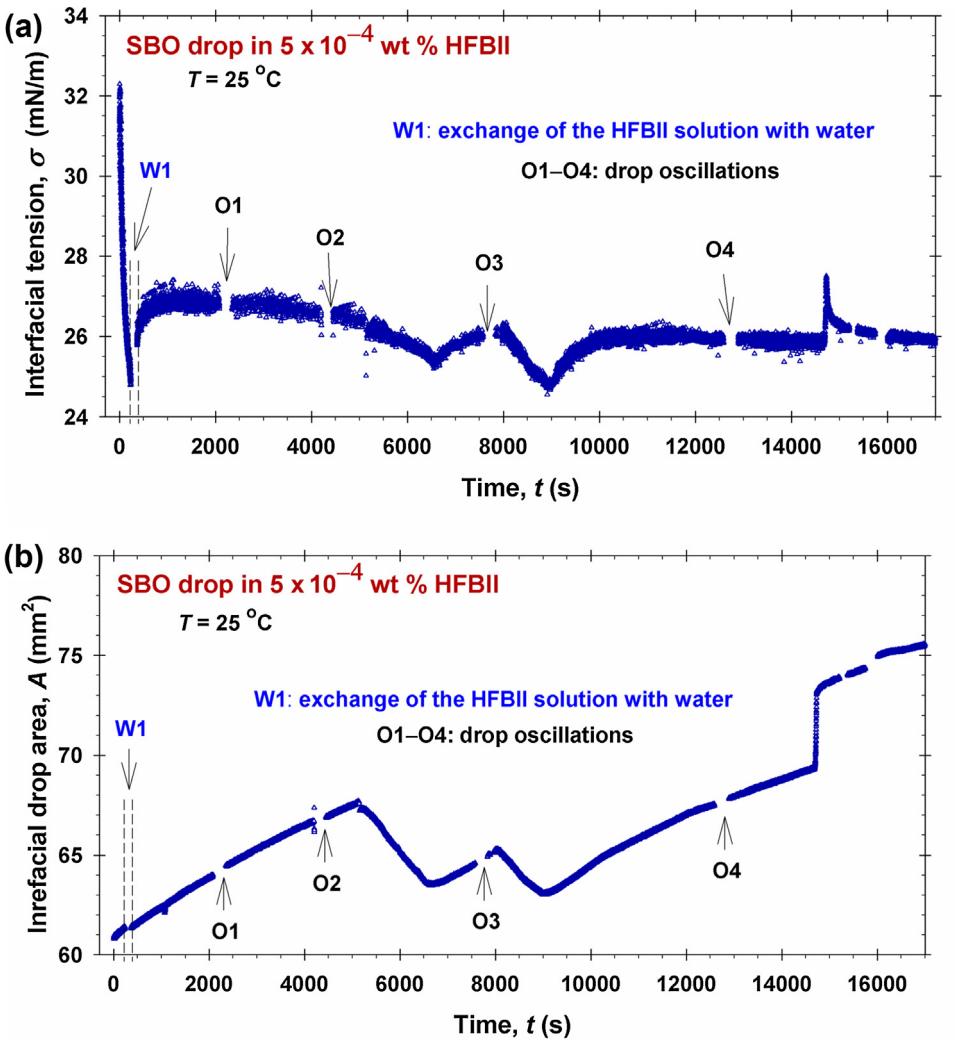

Fig. 2. Data obtained by DSA with drop oscillations for a drop of SBO (in aqueous phase) covered with HFBII adsorption layer. (a) Interfacial tension, σ, vs. time, t. (b) Drop surface area, A, vs. time, t. W1 denotes the time interval, during which the initial 5×10^{-4} wt% HFBII solution was exchanged with water. O1–O4 denote time intervals, during which small drop-surface oscillations were applied to measure the interfacial dilatational moduli, E' and E''.

interface (Fig. 2a). Next, the HFBII solution around the drop (in the working cuvette) is exchanged with water during a relatively short interval of time denoted W1 in Fig. 2. Thus, the adsorption of HFBII is ceased and further decrease of σ is prevented. It is important to note that $\sigma > \sigma^* \approx 21$ mN/m in Fig. 2a. In other words, we are working in the region of fluid HFBII adsorption layers, where the DSA technique is applicable (see Section 4.1). In this experiment, the water phase contains salt at a relatively low concentration, 3 mM NaCl, just to have a defined ionic strength. The oil drop surface area, A, undergoes small and slow occasional variations, which are recorded by the DSA apparatus and shown in Fig. 2b for the respective experiment.

The exchange of the HFBII solution with water (W1 in Fig. 2) is realized by using a cartridge pump, which simultaneously supplies water and sucks out the HFBII solution with the same flow rate, thus keeping the volume of liquid in the working cuvette constant; details can be found in Ref. [71]. After the phase exchange, desorption of HFBII from the surface of the oil drop into the surrounding water phase is possible. To check whether this really happens, we continued the measurement of σ vs. t. Small oscillations of the drop volume (and surface area), denoted O1–O4 in Fig. 2, were applied to determine the interfacial dilatation storage and loss moduli, E' and E'', at different times of contact of the HFBII adsorption layer with the water phase; see Ref. [51] for details about the used method.

Table 2
Experimental data obtained in the oscillating-drop experiments O1–O4 (Fig. 2); details in the text.

Oscillations	Period (s)	E' (mN/m)	E'' (mN/m)	A (mm^2)	σ (mN/m)
O1	2	66.0	0	63.9	26.5
	5	65.9	2.1	64.1	26.5
	10	63.8	4.9	63.9	26.4
O2	2	57.2	0	66.6	26.4
	5	56.4	1.2	66.4	26.4
	10	55.5	4.8	66.8	26.4
O3	2	83.0	0	64.5	25.9
	5	82.3	3.1	64.7	25.9
	10	78.6	5.3	64.7	25.9
O4	2	37.3	0	74.7	26.0
	5	37.5	1.2	74.3	26.0
	10	36.8	3.4	74.5	25.9

The obtained values of E' and E'', are shown in Table 2, together with the used period of drop oscillations and the respective *mean* values of A and σ during the respective oscillatory run. The determined values of the storage modulus, $55 < E' < 83$ (mN/m), are typical for protein adsorption layers. For comparison, for a dense surfactant adsorption layer on the surface of 1 mM SDS solution,

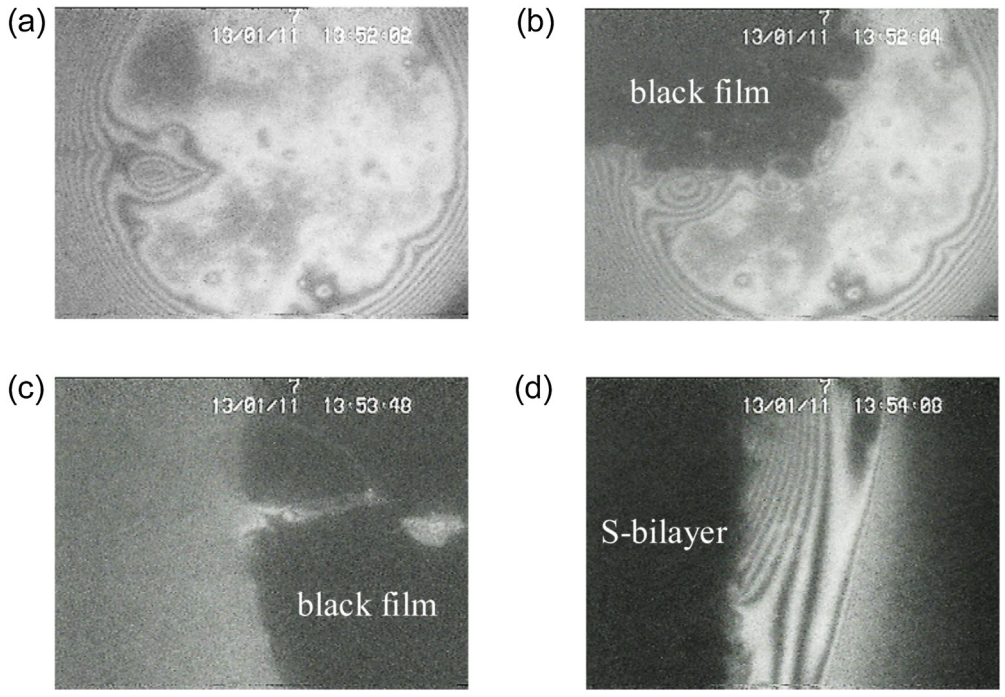

Fig. 3. Evolution of an o/w/o emulsion film formed from 0.005 wt% HFBII aqueous solution; the oil is SBO: (a) During the first 10 min after its formation the film is thick, of non-uniform thickness owing to sandwiched protein aggregates. (b) Next, a spot of 12 nm thick black film appears and fast expands. (c) The black film occupies the whole film area (the brighter zone is the Plateau border). (d) A minute later, sudden transition to 6 nm thick S-bilayer occurs, which is accompanied by a fast and considerable expansion of the film area. The horizontal length of each photo corresponds to 300 μm.

E' = 2.7 mN/m was measured [71]. The high values of E' in Table 2 indicate that there is no HFBII desorption in the water phase during the time of the experiment, 17000 s (4 h and 43 min). Thus, we can conclude that the adsorption of HFBII at the *oil/water* interface is *irreversible*, at least during this period of time. Similar result was obtained for the HFBII adsorption layer at the *air/water* interface in experiments with oscillating bubbles [7].

The smaller values of E' for run O4 (Table 2) are more likely due to the greater drop surface area A for this run, rather than to HFBII desorption. The small values of the loss modulus, E'', as compared to E', indicate that the protein adsorption layer behaves as a predominantly elastic (rather than viscous) body.

We should also note that in the case of irreversible adsorption, there are no equilibrium adsorption and surface-tension isotherms, $\Gamma = \Gamma(C)$ and $\sigma = \sigma(C)$, where Γ and C denote the protein adsorption and bulk concentration, respectively. However, there is two-dimensional equation of state, $\sigma = \sigma(\Gamma)$. To determine the form of this equation, one should measure not only $\sigma(t)$, but also $\Gamma(t)$, however this task is out of the scope of the present study.

The values of σ in Table 2 correspond to surface pressure π_s = 4.5–5.1 mN/m and dilatational storage modulus in the range $55 < E' < 83$ (mN/m). For HFBII adsorption layers at the *air*/water interface, close E' values have been measured for the same π_s; see Fig. 10a in Ref. [7]. Hence, most probably there are no significant differences between the structure of the HFBII adsorption layers at the oil/water and air/water interfaces. This conclusion is confirmed by the fact that S-bilayer is formed in both cases (see Section 5).

5. Emulsion films stabilized with HFBII

Experiments with o/w/o emulsion films stabilized with HFBII were performed by the SE capillary cell. The HFBII concentration was varied from 10^{-4} to 10^{-2} wt% at the solutions' natural pH value, which is 6.0. These experiments give us information about the film thickness and structure (incl. captured aggregates), and about the thinning dynamics of the films and their stability.

At the lowest studied concentration, 10^{-4} wt% HFBII, the emulsion films were not stable – their lifetime was about 1–2 min. At a higher concentration, 10^{-3} wt% HFBII, the films were stable and did not rupture during the time of the experiment (longer than 30 min). The film thinning was quite similar to that of foam films stabilized with HFBII [20]. About a minute after the film formation, a quick transition to S-bilayer was observed; see Fig. A.3 in Appendix A. The S-bilayer represents a film of thickness h = 6 nm, which is composed of two layers of HFBII molecules, whose hydrophobic parts are facing the oil phases, whereas their hydrophilic parts are situated in the middle of the film. The S-bilayer is formed upon direct contact of the protein adsorption layers on the two film surfaces at the end of film thinning. At both 10^{-4} and 10^{-3} wt% HFBII, there was no effect of surface ageing – after waiting for 60 min (before bringing the adsorption layers in contact) the film behavior was the same as with fresh surfaces.

Fig. 3 illustrates the evolution of emulsion films stabilized with 5×10^{-3} wt% HFBII. Much more protein aggregates are seen in the films, as compared to the case with 10^{-3} wt% HFBII. Initially, the films thin relatively slow. About 10 min after the film formation (Fig. 3a), a spot of black film of thickness 12 nm appears and expands (Fig. 3b). Within a minute, the whole film area is occupied by this black film (Fig. 3c). After that, a transition to S-bilayer of thickness 6 nm occurs (Fig. 3d).

At the highest studied protein concentration, 10^{-2} wt% HFBII, the film behavior was very similar to that at 5×10^{-3} wt%, with the only difference that the film thinning occurred considerably slower because of the greater amount of sandwiched protein aggregates. Thus, the spot of fast expanding black film of thickness 12 nm appeared about 50 min after the film formation (against 10 min for 5×10^{-3} wt%). About 5 min later, a transition to S-bilayer is observed.

For all studied protein concentrations, the transition to S-bilayer occurs very fast and is accompanied with a significant growth of the film area (only a small part of the bilayer is seen in Fig. 3d). This happens with both foam and emulsion films stabilized by hydrophobin, and indicates the existence of a strong attraction between the hydrophilic parts of the HFBII molecules in the middle of the film. This attraction leads to decrease of the energy of the system, which favors the growth of film area. All previous observations of S-bilayer have been carried out with *foam* films [9,20,25]. Here, for the first time we report that S-bilayer can form also with *emulsion* films (Fig. 3c).

At 5×10^{-3} and 10^{-2} wt% HFBII, if we keep the two film surfaces separated for 60 min before bringing them in contact, formation of S-bilayer is not observed. Such films contain a significant amount of sandwiched protein aggregates that serve as spacers and block the further film thinning. During the waiting period of 60 min, aggregates have been growing in the solution and a part of them has adhered to the film surfaces. After that, they have not been driven out of the film by the hydrodynamic flow during the film thinning.

6. SBO-in-water emulsions stabilized by HFBII

6.1. Photographs of the produced emulsions

SBO-in-water emulsions have been prepared at three volume fractions of oil, $\Phi_{oil} = 0.10$, 0.30 and 0.50, and at protein concentrations, C_{HFBII}, between 0.05 and 7 wt% HFBII in the aqueous phase. As an illustration, we compare photographs of an emulsion prepared at $\Phi_{oil} = 0.30$ and $C_{HFBII} = 0.1$ wt% (Fig. 4) with analogous photographs of an emulsion prepared at $\Phi_{oil} = 0.10$ and $C_{HFBII} = 0.5$ wt% (Fig. 5). After the first homogenization (for 3 min at 12 000 rpm), most of the formed oil drops are non-spherical (ellipsoidal) of size greater than 20 μm (Figs. 4a and 5a). After the second emulsification (for 5 min at 24 000 rpm) the average size of the drops is markedly smaller. For $\Phi_{oil} = 0.30$, the drops are *spherical* (Fig. 4b), whereas for $\Phi_{oil} = 0.10$, the drops are *ellipsoidal* (Fig. 5b). After storage for several days, no significant changes have been detected in the investigated emulsions: the emulsion drops have preserved their size and shape (Figs. 4c and 5c). In particular, for $\Phi_{oil} = 0.10$ the drops have remained ellipsoidal and adhesion of the small drops to the surfaces of the big drops is observed (Fig. 5c). This is not surprising in view of the sticky interactions detected in the experiments with thin emulsion films (Section 5).

During emulsification, a relatively small number of air bubbles could be formed. Due to the action of buoyancy force, they emerge in the upper layer of the emulsion, where they are observed as darker objects in the fresh emulsions (Fig. 5b), or as wrinkled spheroidal objects after longer storage (Fig. 5c); see also Ref. [19].

For a fluid protein adsorption layer at the oil/water interface, the equilibrium drop shape is the spherical one. Consequently, any deviation from the spherical shape indicates *solidification* of the interfacial adsorption layer; see e.g. [20,72]. In our case, such solidification happens at sufficiently high surface concentrations of HFBII; see Fig. 1. This is fulfilled for Fig. 4a, where the drops are bigger and the interfacial area is smaller, and for Fig. 5, where the protein adsorption is greater because of the higher HFBII concentration and lower oil volume fraction. In contrast, for Fig. 4b and c a smaller amount of protein is distributed over a greater interfacial area, which has led to the formation of fluid HFBII adsorption layers, as evidenced by the spherical shape of the drops.

6.2. Drop size distributions and their interpretation

Information about the emulsification regime can be obtained from the size distribution of the emulsion drops. Illustrative size distributions determined at different protein concentrations and at fixed $\Phi_{oil} = 0.30$ are shown in Fig. 6, and at fixed $\Phi_{oil} = 0.10$ – in Fig. 7. In particular, the distributions in Fig. 6a and b are broad with indications for two peaks (bimodal distributions). These two distributions correspond to lower protein adsorption on the drop surfaces and are result from emulsification in regime of *limited coalescence* (see below).

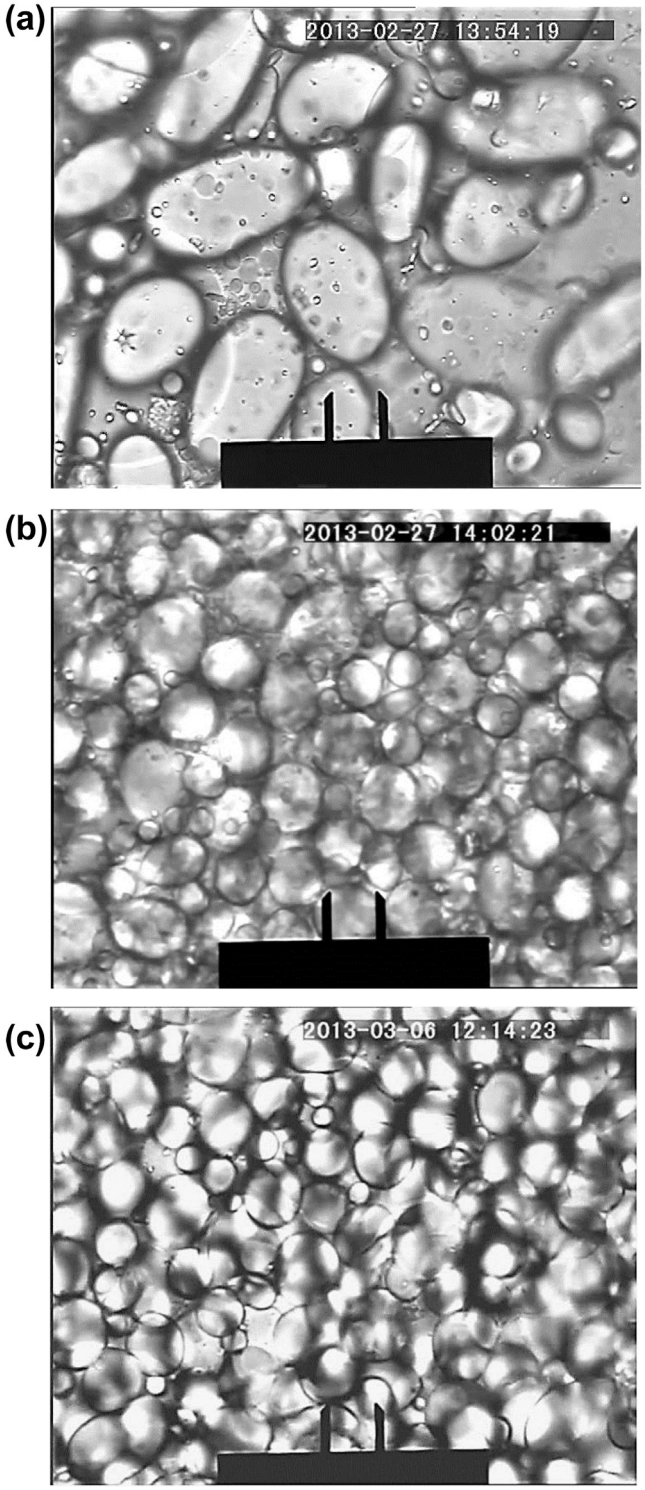

Fig. 4. $\Phi_{oil} = 0.30$, $C_{HFBII} = 0.1$ wt%. Photographs of a SBO-in-water emulsion obtained as follows: (a) Homogenization for 3 min at 12 000 rpm. (b) After a subsequent homogenization for 5 min at 24 000 rpm. (c) After 7 days storage in fridge at 4 °C. (reference mark = 20 μm).

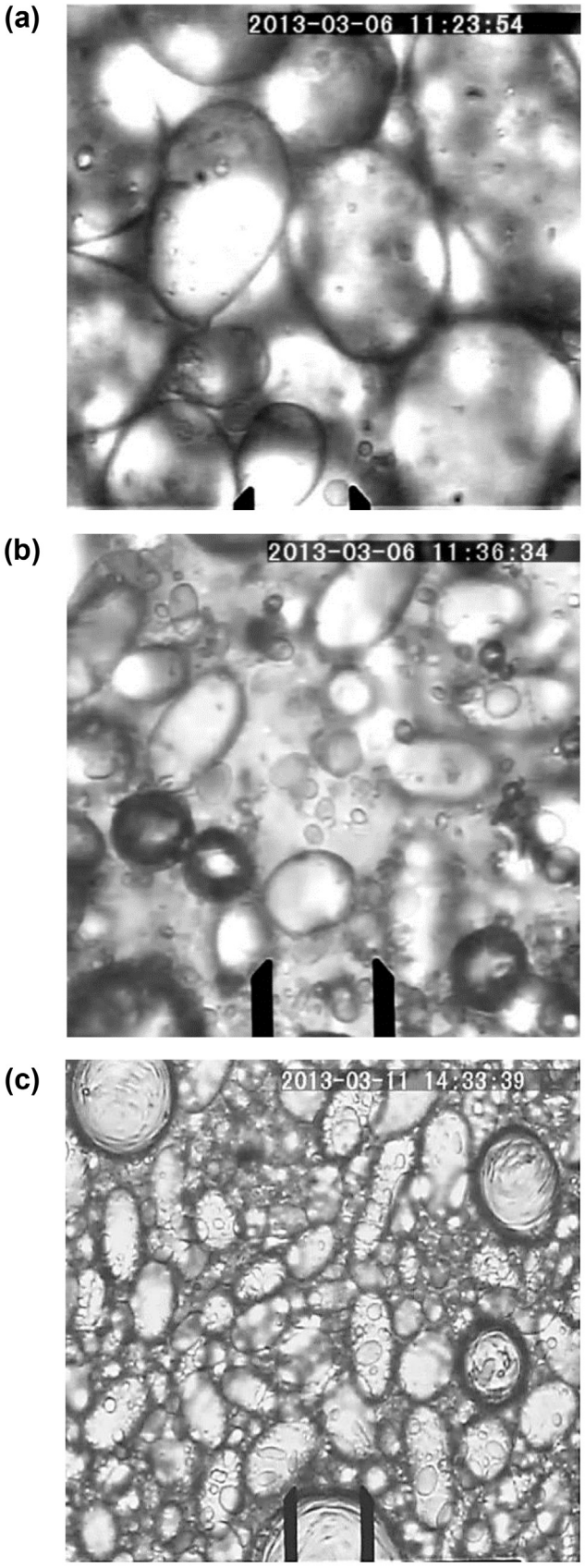

Fig. 5. $\Phi_{oil} = 0.10$, $C_{HFBII} = 0.5$ wt%. Photographs of a SBO-in-water emulsion obtained as follows: (a) Homogenization for 3 min at 12 000 rpm. (b) After a subsequent homogenization for 5 min at 24 000 rpm. (c) After 5 days storage in fridge at 4 °C. (reference mark = 20 μm).

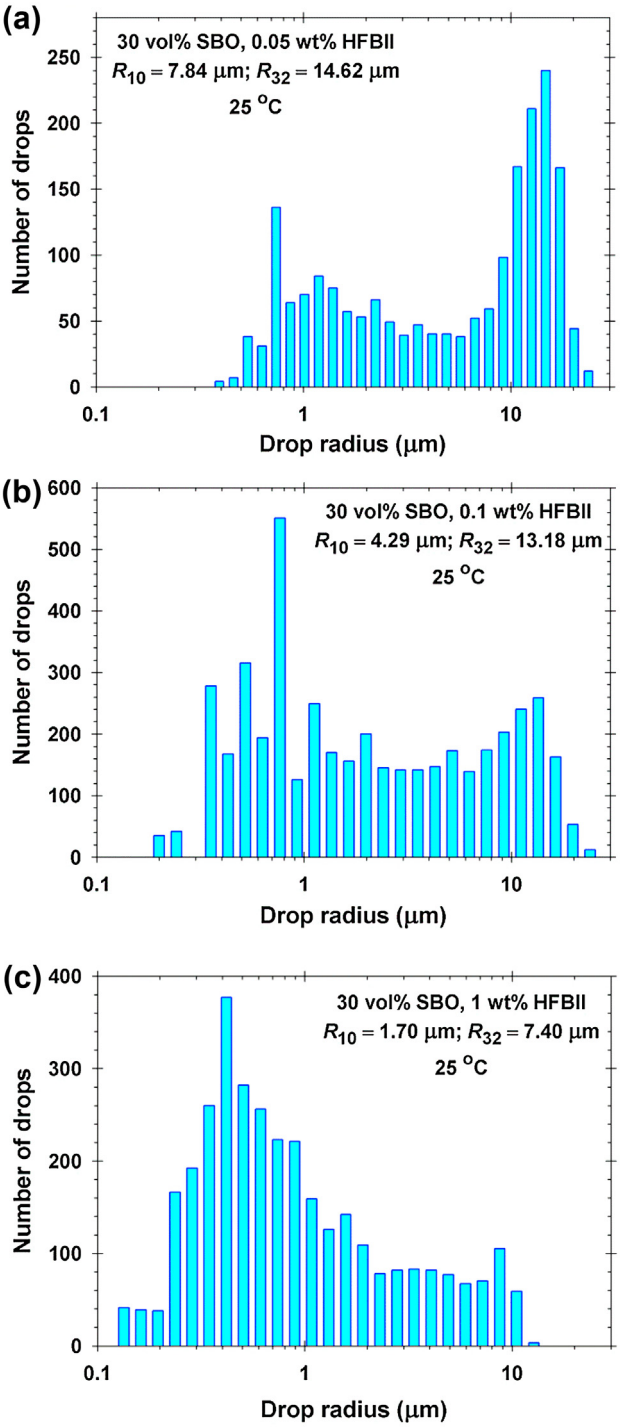

Fig. 6. $\Phi_{oil} = 0.30$. Drop-size distribution in the investigated SBO-in-water emulsions at different HFBII concentrations in the aqueous phase: (a) 0.05 wt%; (b) 0.1 wt% and (c) 1 wt%.

In contrast, the distributions in Figs. 6c and 7 possess a well pronounced peak in the zone of the smaller drops and a "tail" in the zone of the bigger drops. These distributions correspond to higher protein adsorptions on the surfaces of the produced drops and are result from emulsification in the *Kolmogorov regime* (see below).

As seen in Fig. 6, the smallest drop radii measured from video frames of the diluted emulsions are about 0.2 μm. Indeed,

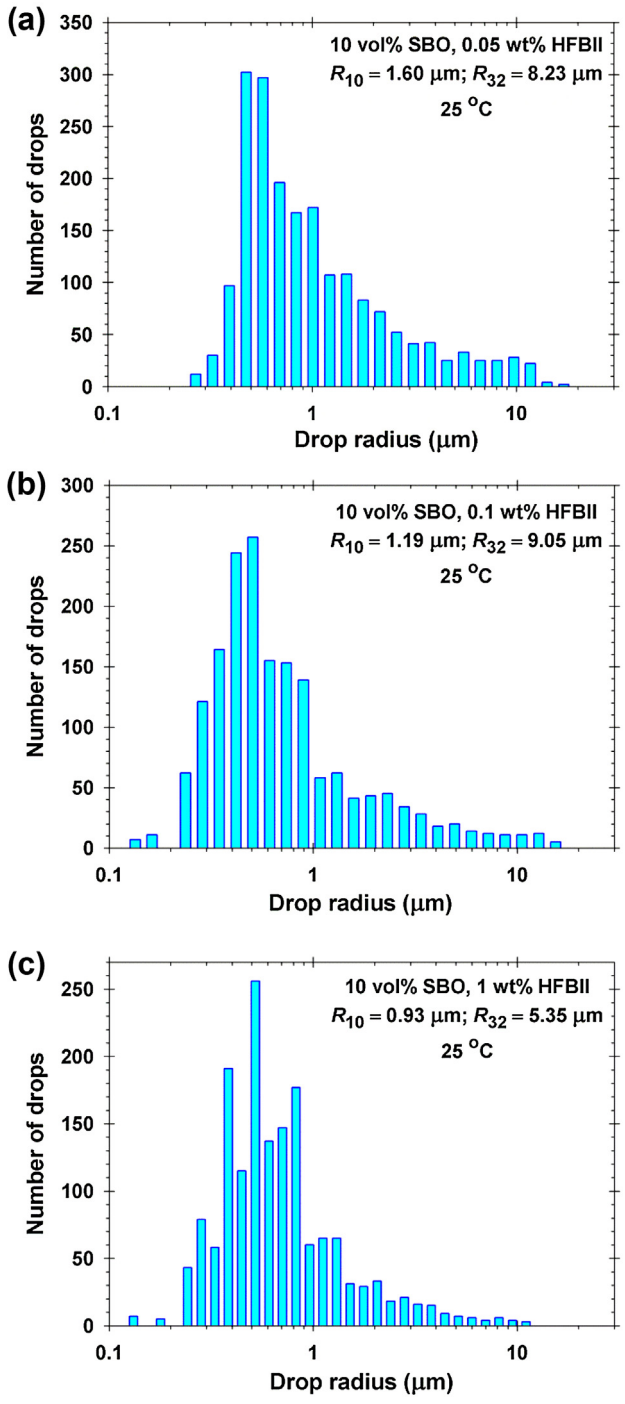

Fig. 7. Φ_{oil} = 0.10. Drop-size distribution in the investigated SBO-in-water emulsions at different HFBII concentrations in the aqueous phase: (a) 0.05 wt%; (b) 0.1 wt% and (c) 1 wt%.

according to the Rayleigh criterion the diameter of the objects visible by optical microscopy is [73]:

$$2R \geq 0.61\frac{\lambda}{NA} \tag{13}$$

Here, λ is the wavelength of light and *NA* is the numerical aperture of the objective. Substituting typical parameter values for visible light in Eq. (13), λ = 490 nm and *NA* = 1.5, for the minimal drop diameter we obtain $2R_{min} \approx 0.2$ μm, in accordance with our observations (Fig. 6).

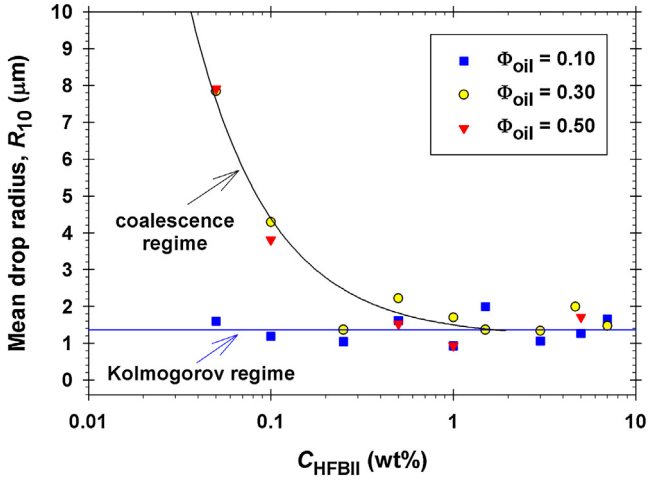

Fig. 8. Plot of R_{10} vs. the hydrophobin concentration in the aqueous phase, C_{HFBII}, for three different values of the oil volume fraction, Φ_{oil}, denoted in the figure.

From the drop size distributions we calculated the mean drop radius R_{10} using Eq. (1). In Fig. 8, the obtained values of R_{10} are plotted vs. the input HFBII concentration in the aqueous phase, C_{HFBII}, for three different oil volume fractions in the emulsion: Φ_{oil} = 0.10, 0.30 and 0.50. Each point in Fig. 8 represents the value of R_{10} calculated from the measured radii of at least 1000 drops in the respective emulsion; see Eq. (1). The standard error of R_{10}, given in Table A1 in Appendix A, is smaller than the size of the symbols in Fig. 8. The scattering of the data in Fig. 8 is due to an inherent irreproducibility of the emulsification experiments. The standard error of R_{32} (which is greater than that of R_{10}) is shown in Fig. 9a and b.

As seen in Fig. 8, at Φ_{oil} = 0.10 the mean drop radius is independent of protein concentration. This indicates emulsification in the Kolmogorov regime. In other words, the number of the oil drops produced in the turbulent flow is small enough so that the available protein stabilizes all of them by forming dense adsorption layers on their surfaces. In this regime, R_{10} is determined by the mechanical power of the homogenizer, ε; see Eqs. (10) and (11). Because the experimental conditions, including the drop size and viscosity of oil, are similar to those used in Ref. [65], we may expect that the emulsification occurs in the inertial regime, as established there.

For Φ_{oil} = 0.30 and 0.50, at the higher concentrations ($C_{HFBII} \geq 0.5$ wt%) R_{10} approaches the same constant value as for Φ_{oil} = 0.10 (Fig. 8), which again indicates emulsification in the Kolmogorov regime. However, at $C_{HFBII} \leq 0.1$ wt% the values of R_{10} are significantly greater, which indicates emulsification in the limited coalescence regime at the lower protein concentrations.

To check that, from the drop size distributions we calculated R_{32} using Eq. (1). In Fig. 9a and b, the obtained values of R_{32} are plotted vs. $1/C_{HFBII}$ in accordance with Eq. (8). The data plots show that the dependence of R_{32} on $1/C_{HFBII}$ agrees well with a straight line of *nonzero* intercept. In view of Eq. (8), such dependence can be explained if the mean size of the protein aggregates increases linearly with the protein concentration:

$$a_{32} = a_1 + a_2 C_{HFBII} \tag{14}$$

Then, Eq. (8) acquires the form:

$$R_{32} = \frac{4\rho_{HFBII}}{\rho_{sol}}\frac{\Phi_{oil}}{1-\Phi_{oil}}\left(a_2 + \frac{a_1}{C_{HFBII}}\right) \tag{15}$$

The parameters a_1 and a_2 determined from the fits of the data in Fig. 9a and b with linear regressions are given in Table 3. The obtained values of a_1 are of the order of the radius of a HFBII molecule or oligomer, which is a reasonable result. To illustrate

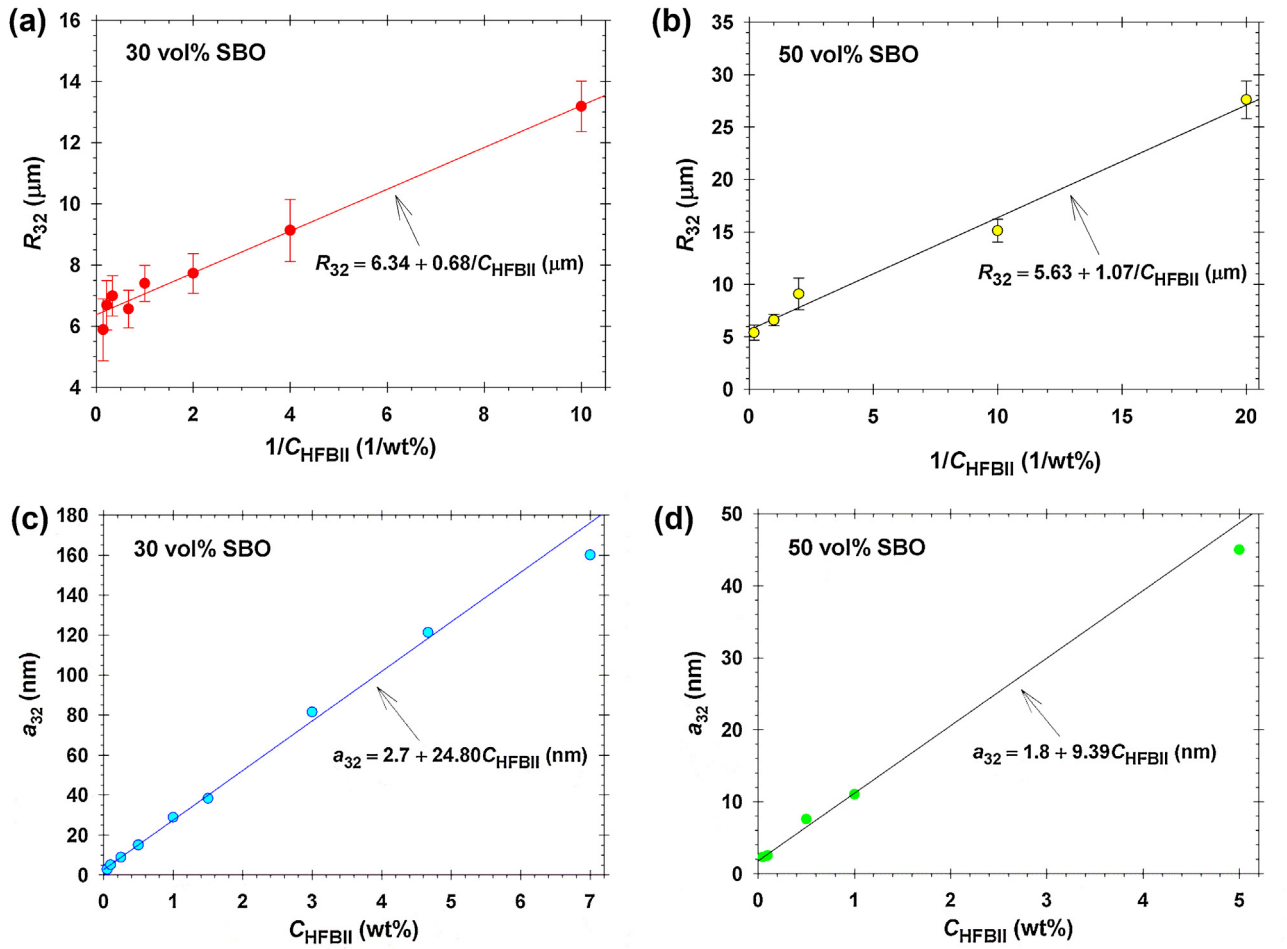

Fig. 9. Plots of R_{32} vs. $1/C_{HFBII}$ for (a) Φ_{oil} = 0.30 and (b) Φ_{oil} = 0.50, and plots of a_{32} vs. C_{HFBII} for (c) Φ_{oil} = 0.30 and (d) Φ_{oil} = 0.50.

Table 3
Values of the parameters a_1 and a_2 in Eq. (14) obtained from the data fits in Fig. 9a and b with linear regressions in accordance with Eq. (15).

Φ_{oil}	a_1 (nm)	a_2 (nm/wt%)
0.30	2.7 ± 1.5	24.8 ± 0.6
0.50	1.8 ± 0.2	9.4 ± 1.0

the variation of the aggregate size with the protein concentration, in Fig. 9c and d we have plotted the values of a_{32} obtained from the respective R_{32} in Eq. (8); the solid lines present graphically Eq. (14) with a_1 and a_2 from Table 3.

We recall that a_{32} is the mean radius of the protein aggregates that have been adsorbed *at the drop surfaces*. From this viewpoint, it is not surprising that a_2 is smaller for the higher oil volume fraction, Φ_{oil} = 0.50. A possible explanation can be the following. During the homogenization, the turbulence leads to both drop-aggregate and aggregate–aggregate collisions. The former may result in aggregate adsorption, whereas the latter – in the formation of bigger aggregates. At the higher Φ_{oil}, there are more drops and the uptake of protein aggregates is more probable, which reduces the concentration of free aggregates and the probability of their flocculation upon the collisions between them.

6.3. Stability of the emulsions with HFBII

Drop size distributions have been determined at different storage times, up to 50 days (in fridge at 4 °C). The results show that the drop-size distribution in a given emulsion does not vary with the storage time. As emulsifier, HFBII provides a high stability of the emulsions upon storage. Moreover, if the drops in the emulsions with HFBII have been initially elongated (rather than spherical), the elongated shape does not relax to spherical one even after 50 days of storage.

Thus, the emulsions with HFBII are stable rest. However, if such an emulsion is subjected to stirring, then drop coalescence and breakage of the emulsion is observed. For example, if we try to disperse the droplets of a HFBII-stabilized emulsion in pure water by stirring, the emulsion is destroyed. In this experiment, a portion of the cream-like emulsion was put in a test tube with water. Four–five shakes (by hand) led to breakage of the emulsion and phase separation, which happened fast, within 30 s. This is a rather surprising result, because the HFBII adsorbs irreversibly at the oil-water interface (see Section 4.2), and it does not desorb in the water phase. Indeed, as seen in Fig. 2a and Table 2, there are no indications for HFBII desorption from the oil/water interface during a period of 17,000 s (4 h 43 min).

The fact that the emulsions with HFBII are stable for months at rest, but they are easily destroyed when subjected to shear stress, implies that we are dealing with solidified, but fragile protein adsorption layers on the drop surfaces. Moreover, the formation of S-bilayer observed in the thin-film experiments (Section 5) and the photographs of the emulsions (like Fig. 5c) indicate that the emulsion drops covered with HFBII layers are sticky and may form flocs. It seems that the fragile network of protein adsorption layers (ca. 3 nm thick) in such an emulsion break when subjected to the action

of shear stresses and the encapsulated oil is released. Unlike the fluid adsorption layers, the cracks and voids in a solidified protein film cannot be repaired by release and surface transport of protein molecules from the domains covered with two-dimensional condensed (solidified) phase of protein.

The mechanism of emulsion destruction in shear flow might find application for cargo release from hydrophobin-stabilized microcapsules. The detailed investigation of this mechanism could be a subject of subsequent study.

In our experiments, to prevent the drop coalescence during the drop-size measurements, the emulsions were diluted with a 5 mM SDS solution before stirring. The obtained diluted emulsions were stable, which means that the drop-size distribution is preserved and it represents the drop-size distribution in the original, non-diluted HFBII stabilized emulsion. Moreover, in the presence of SDS the HFBII-covered drops become spherical (rather than ellipsoidal or irregularly shaped), which makes easy and accurate the determination of their diameter, surface area and volume.

Another way to prevent the strong drop–drop adhesion is to cover the HFBII coated drops with a less adhesive second layer from another protein, e.g. BLG. Results for the stability of emulsions from mixed solutions of HFBII and BLG are presented in the next section.

7. Emulsions from mixed solutions of HFBII and BLG

In these experiments, the SBO volume fraction was 30 vol% and the total protein concentration was 0.25 wt% for all studied emulsions. The proteins, HFBII and BGL, were simultaneously dissolved in water, the soybean oil was added, and the mixture was subjected to homogenization.

7.1. Emulsion stability upon centrifugation

The prepared fresh emulsions were subjected to centrifugation at 25 °C for 6 h at a centrifugal acceleration of 4000*g*. The height of the oil layer released above the emulsion was measured by an electronic micrometer.

In Fig. 10a, the volume of the released oil, V_{rel}, scaled with the total volume of the oil phase, V_{tot}, is plotted as a function of the weight fraction of HFBII in the mixture with BLG:

$$X_{HFBII} = \frac{w_{HFBII}}{w_{HFBII} + w_{BLG}} \quad (16)$$

where w_{HFBII} (w_{BLG}) is the weight of HFBII (BLG) dissolved in the aqueous phase. As seen in Fig. 10a, for $X_{HFBII} \leq 0.1$ about 30% of the oil was released upon centrifugation. In other words, if BLG is the predominant component in the protein blend, then the produced emulsions are the most unstable. In the opposite case, for emulsions stabilized by HFBII alone ($X_{HFBII} = 1$) the volume of the released oil is 10% of the total amount of oil. The most stable (upon centrifugation) are the emulsions corresponding to the interval $0.33 \leq X_{HFBII} \leq 0.50$, where only 4.3% of the oil was released. In this respect, the mixing of HFBII and BLG has a *synergistic* effect.

7.2. Emulsion stability upon stirring

This experiment was carried out with an emulsion at $X_{HFBII} = 0.33$. A portion of the emulsion was placed into a flask with pure water and stirring was applied to disperse the emulsion drops. A *stable* diluted emulsion was obtained. (We recall that at $X_{HFBII} = 1$ similar dilution and stirring leads to destabilization of the emulsion; see Section 6.3). In the photos of the diluted emulsion deformed, non-spherical drops are seen, which evidences surface solidification; see Fig. A.4 in Appendix A.

In Ref. [9], it was established that the more surface active HFBII occupies the interface, whereas BLG forms a second adsorption

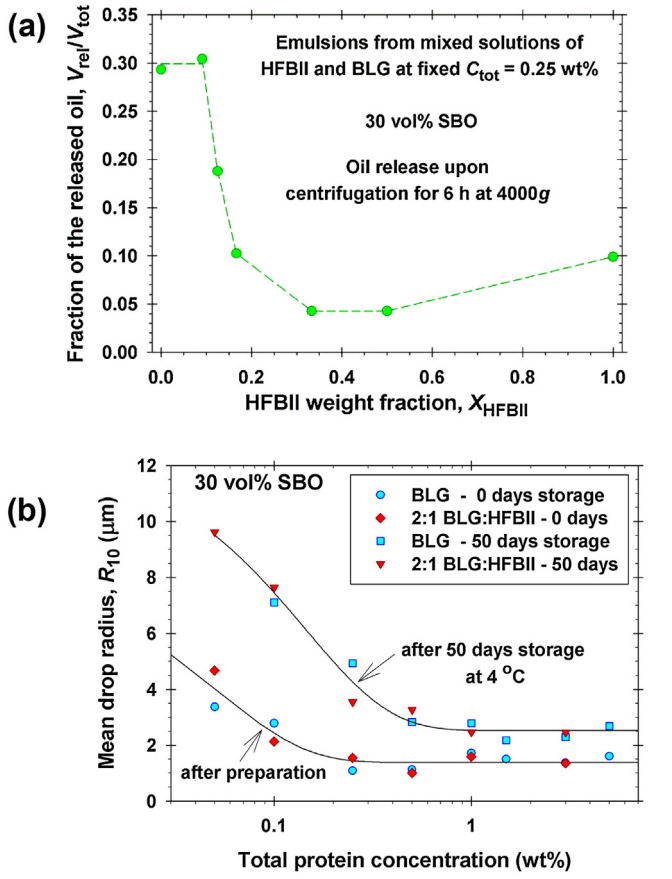

Fig. 10. Data for SBO-in-water emulsions at 30 vol% SBO. (a) Volume of the released oil upon centrifugation scaled with the total oil volume, V_{rel}/V_{tot}, vs. the hydrophobin weight fraction, X_{HFBII}, in mixed aqueous solutions of HFBII and BLG at a fixed total protein concentration of 0.25 wt%. (b) Plots of the mean drop radius R_{10} vs. the total protein concentration – comparison of results for emulsions stabilized by BLG alone and 2:1 BLG/HFBII immediately after their preparation and after 50 days of storage at 4 °C.

layer adjacent to the monolayer of hydrophobin. In such a case, the adhesion between the BLG-covered emulsion drops would be much weaker. Indeed, the contact angle of a thin film stabilized with HFBII (two adherent hydrophobin adsorption layers) could reach 51°, whereas for regular proteins, like BLG, the contact angle does not exceed 7° [25], i.e. the second layer of BLG can prevent the drop–drop adhesion. Moreover, the second layer of BLG can serve as a source of protein molecules that can fill the cracks and voids in the solidified HFBII adsorption layer that appear when the emulsion drops are deformed under the action of shear stresses. This could explain the synergistic (stabilizing) effect of the mixed adsorption layers from HFBII and BLG (Fig. 10a).

A possible reason for the formation of a second layer of BLG, which is adherent to the HFBII adsorption layer, could be the presence of *patch-charge attraction* between the BLG and HFBII molecules. This is electrostatic attraction between oppositely charged patches on the surfaces of two protein molecules [74]. There are indications that patch-charge attraction acts also between the BLG molecules in aqueous solution. Indeed, the fact that pronounced aggregation is observed in BLG solutions at low ionic strengths can be explained with the patch-charge attraction [75]. In our case, the formation of a bilayered adsorption film from HFBII and BLG molecules implies that the BLG–HFBII attraction is weaker than the HFBII–HFBII attraction.

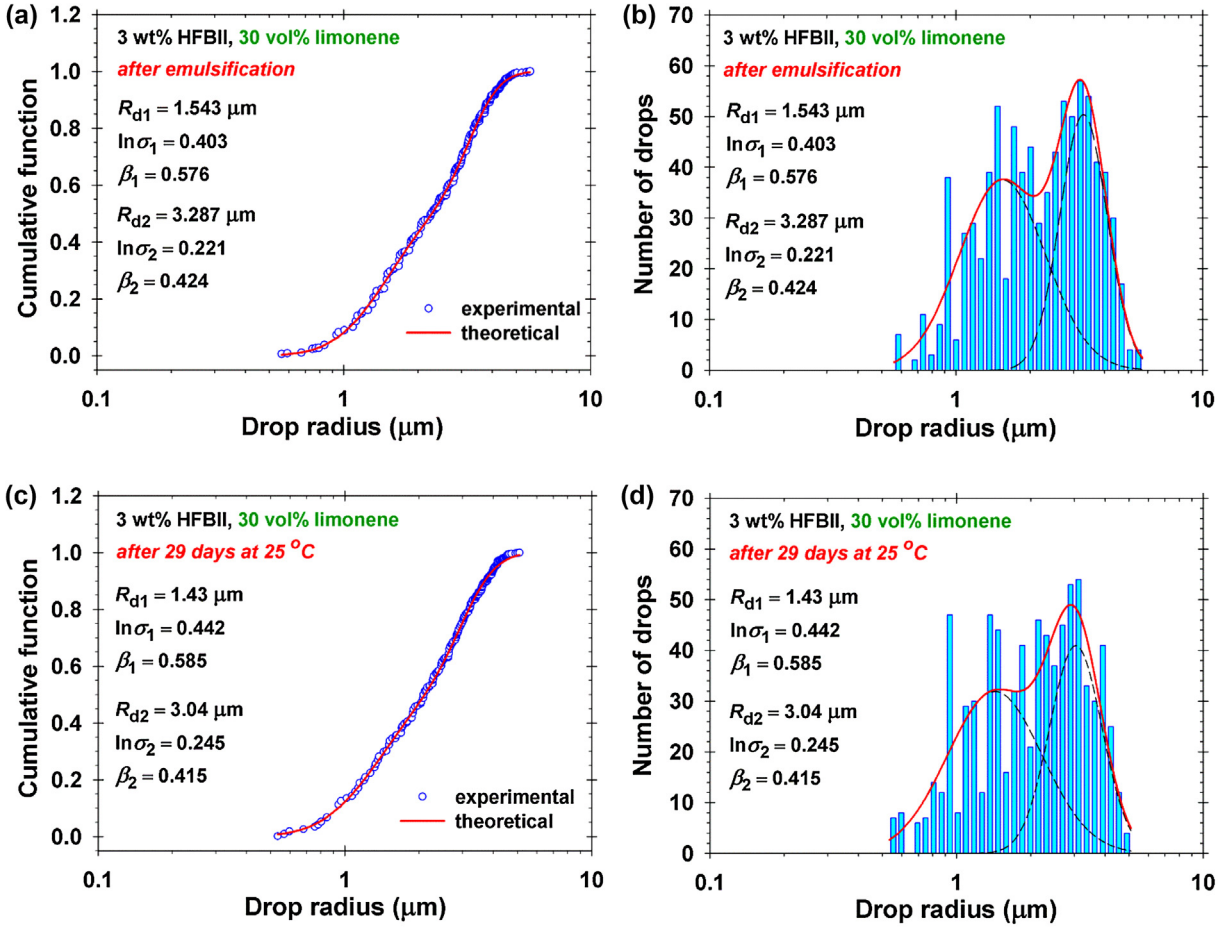

Fig. 11. Data for limonene-in-water emulsions (Φ_{oil} = 0.30) stabilized with 3 wt% HFBII in the water phase. (a and c) Plots of the cumulative function vs. the drop radius and (b and d) drop-size distributions. The solid line represents the best fit with a bimodal lognormal distribution for the data after 0 and 29 days of storage at 25 °C. The dashed lines show the two constituent unimodal distributions. There are no indications for Ostwald ripening.

7.3. Emulsion stability upon storage

SBO-in-water emulsions stabilized with BLG (instead of HFBII) were investigated at storage times 0, 4, 7, 17, 25, 35 and 50 days at 4 °C. The drops in the emulsions with BLG were spherical (low surface shear elasticity), unlike the emulsions with HFBII, where elongated drops were observed (see above). After storage for 7 days, we observed oil lenses and/or spread oil layer on the top of the emulsions for all studied BLG concentrations, from 0.05 to 5 wt%. The emulsions with BLG were less stable than those with HFBII, for which no separation of oil was observed.

Drop-size distributions have been obtained at different storage times and the mean drop radii, R_{10} and R_{32}, have been determined. The standard error of R_{10}, given in Table A2 in Appendix A, is smaller than the size of the symbols in Fig. 10b. The scattering of the experimental points is due to the inherent irreproducibility of the emulsification experiments. At storage time t = 50 days, R_{10} is markedly greater than at t = 0; see Fig. 10b. This indicates drop *coalescence* upon storage even at the higher BLG concentrations, ≥1 wt%. (We recall that SBO is practically insoluble in water, so that the increase of R_{10} could not be due to Ostwald ripening.) In HFBII-stabilized emulsions, such coalescence is missing (see above). This is another unique property of HFBII.

SBO-in-water emulsions stabilized with BLG and HFBII at weight ratio 2:1 ($X_{HFBII} \approx 0.33$) have been also investigated at storage times 0, 4, 7, 17, 36 and 50 days at 4 °C. After storage for 50 days, we observed oil lenses and/or spread oil layer on the top of the emulsions for all studied BLG + HFBII concentrations. For the emulsions with BLG alone, this happened on the 7th day, whereas for the emulsions with HFBII alone oil separation was not observed at all. Hence, the emulsions with 2:1 BLG/HFBII have an intermediate stability between those containing BLG or HFBII alone.

The rise of the mean drop radius, R_{10}, after storage of the emulsion for 50 days is almost the same for the emulsions stabilized with BLG alone and with 2:1 BLG/HFBII (Fig. 10b), but such a rise of R_{10} is absent in the case of HFBII alone. Hence, the added BLG determines the mean drop size, but it worsens the long-time stability of the emulsions with HFBII. Note that the inclined and horizontal parts of the lower curve in Fig. 10b are related to the "limited coalescence" and "Kolmogorov" regimes; see Fig. 8.

8. Ostwald ripening in emulsions stabilized by HFBII and other amphiphilic molecules

8.1. Limonene-in-water emulsions

(a) *HFBII:* We investigated limonene-in-water emulsions at three protein concentrations, 0.1, 1 and 3 wt% HFBII at Φ_{oil} = 0.30. Because of the relatively high solubility of limonene in water (13.8 mg/L), we expected that Ostwald ripening could happen in these emulsions. By size and shape (elongated), the drops in the emulsions with limonene and SBO are similar, i.e. the limonene does not prevent the solidification of the hydrophobin adsorption layers.

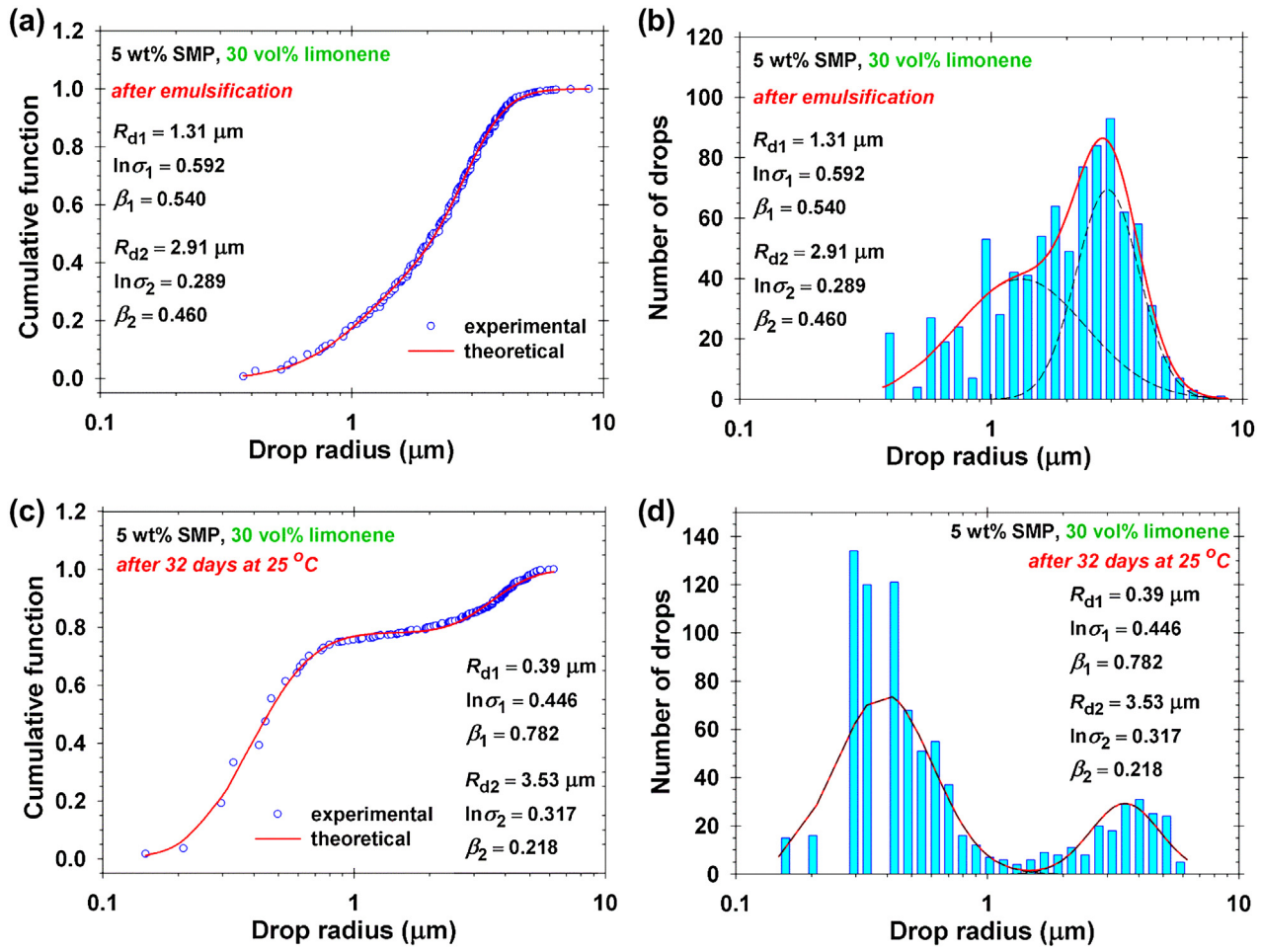

Fig. 12. Data for limonene-in-water emulsions (Φ_{oil} = 0.30) stabilized with 5 wt% SMP in the water phase. (a and c) Plots of the cumulative function vs. the drop radius and (b and d) drop-size distributions. The solid line represents the best fit with a bimodal lognormal distribution for the data after 0 and 32 days of storage at 25 °C. The dashed lines show the two constituent unimodal distributions. The data indicate well pronounced Ostwald ripening.

All emulsions prepared at 0.1, 1 and 3 wt% HFBII were stable upon storage for one month at 25 °C. At 0.1 wt% HFBII, the emulsion was relatively monodisperse with a mean drop radius of 2.2 μm; unimodal lognormal distribution, see Eqs. (4) and (5). At the higher concentrations, the experimental drop-size distributions can be described by the bimodal lognormal law, see Eqs. (6) and (7). The mean drop radii, $R_{d1} \approx 1.5$ μm and $R_{d2} \approx 3.5$ μm, were practically constant for all studied samples of the emulsion taken at different storage times; see Fig. 11. HFBII blocks the Ostwald ripening at all studied protein concentrations.

(b) *BLG:* The emulsions prepared with 0.1 and 1 wt% BLG were unstable because of the occurrence of slow coalescence. Oil lenses were observed on the top of the emulsions after storage for 2 and 7 days. At the highest studied concentration, 3 wt% BLG, the emulsions were stable at least for one month; see Fig. A.5 in Appendix A. BLG blocs the Ostwald ripening at 3 wt% BLG, but this concentration is 30 times higher than the lowest studied HFBII concentration corresponding to stable emulsion (0.1 wt%).

(c) *Tween 20:* The emulsions with 0.016 wt% Tween 20 were unstable – the video records show that slow drop coalescence takes place. At higher concentrations, 0.16 and 0.5 wt% Tween 20, the emulsions were monodisperse and stable upon storage for one month at 25 °C. The mean drop radius decreases from 2 μm to 1.3 μm with the increase of surfactant concentration. Tween 20 blocks the Ostwald ripening at concentrations higher than 0.16 wt%; see Fig. A.7 in Appendix A.

(d) *SMP:* In the presence of 0.1 wt% SMP the emulsions were unstable: after 4 days of storage at room temperature oil lenses were observed on the top of the emulsions. For concentrations above 0.1 wt% SMP, the produced emulsions were stable against coalescence (no release of oil). However, upon storage for one month considerable changes in the drop-size distributions is observed; see e.g. Fig. 12. These changes indicate the occurrence of well pronounced Ostwald ripening at all studied SMP concentrations: 0.5; 1; 5 and 7 wt%; see also Fig. A.6 in Appendix A.

8.2. Xylene-in-water emulsions

At 25 °C the solubility of xylene in water is about 12 times higher than that of limonene. To further accelerate the process of Ostwald ripening, we carried out the experiments with xylene at a higher temperature, 60 °C, at which its water solubility further increases 1.5 times [50]. The oil volume fraction was Φ_{oil} = 0.30, as in the case of limonene.

(a) *HFBII:* At 0.1 wt% HFBII, the produced emulsion was unstable – after 1 h at 60 °C release of oil lenses was observed. At 1 wt% HFBII, the emulsion was unstable after 72 h at 60 °C because of drop coalescence (release of oil lenses). At 3 wt% HFBII, the

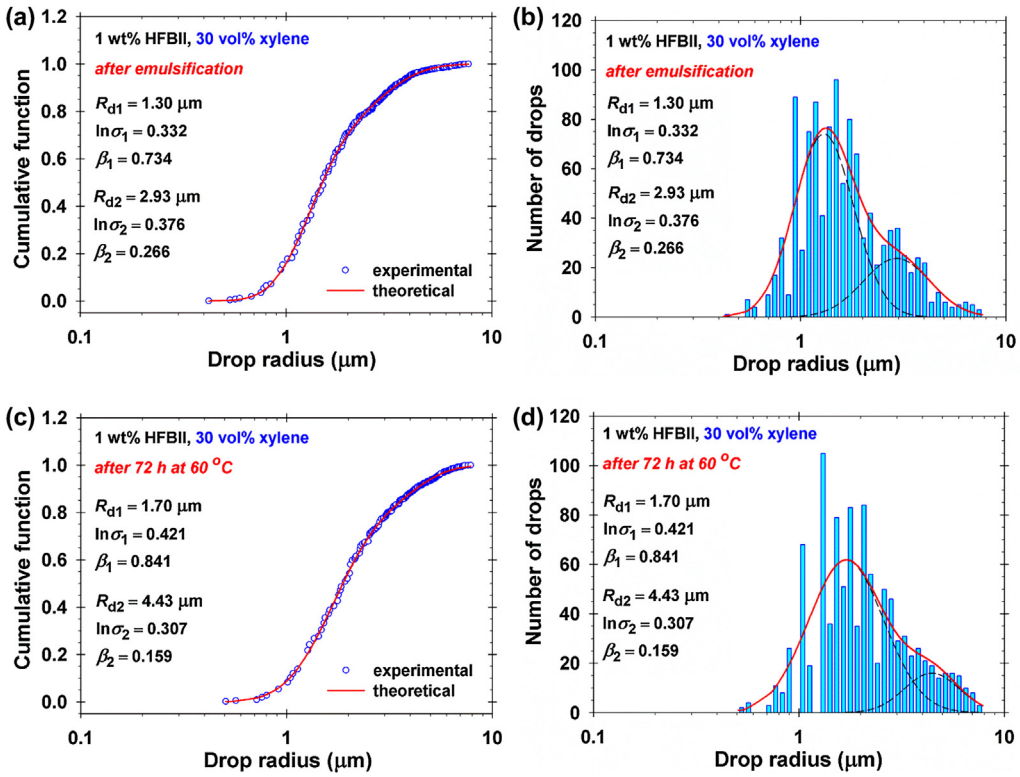

Fig. 13. Data for xylene-in-water emulsions (Φ_{oil} = 0.30) stabilized with 1 wt% HFBII in the water phase. (a and c) Plots of the cumulative function vs. the drop radius and (b and d) drop-size distributions. The solid line represents the best fit with a bimodal lognormal distribution for the data after 0 and 72 h of storage at 60 °C. The dashed lines show the two constituent unimodal distributions. There are no well pronounced indications for Ostwald ripening.

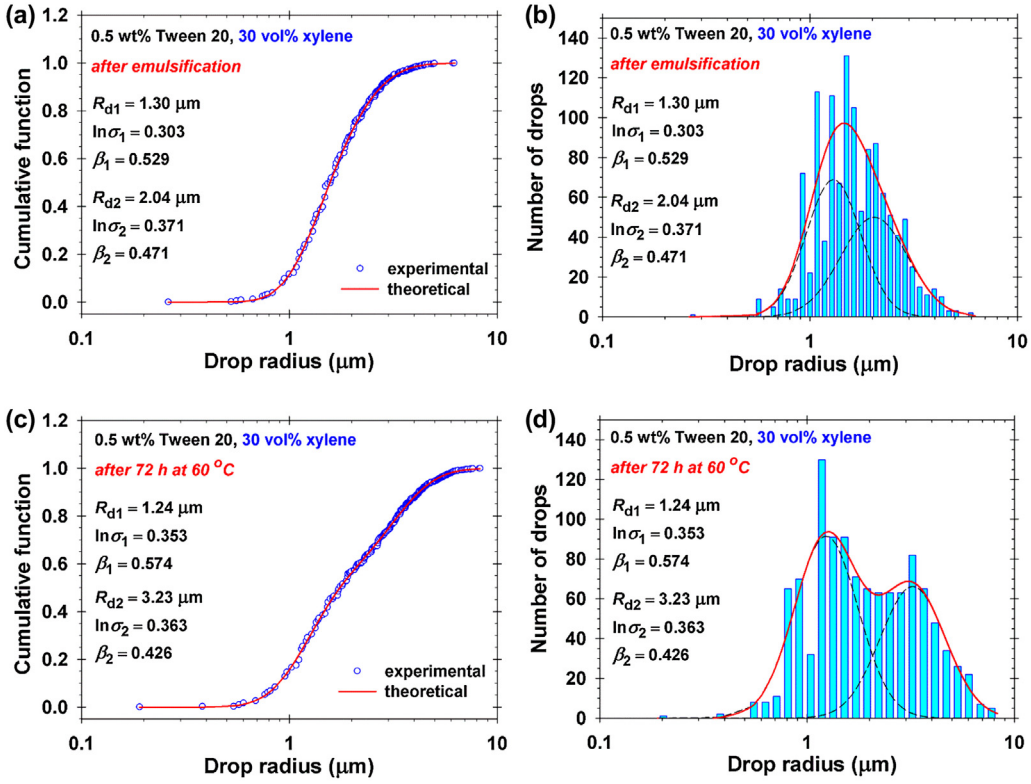

Fig. 14. Data for xylene-in-water emulsions (Φ_{oil} = 0.30) stabilized with 0.5 wt% Tween 20. (a and c) Plots of the cumulative function vs. the drop radius and (b and d) drop-size distributions. The solid line represents the best fit with a bimodal lognormal distribution for the data after 0 and 72 h of storage at 60 °C. The dashed lines show the two constituent unimodal distributions. There are indications for Ostwald ripening.

emulsion was stable after 72 h at 60 °C. At concentrations 1 and 3 wt% HFBII, the drop size distributions don not show any pronounced indications for Ostwald ripening; see Fig. 13.

(b) *Tween 20:* The drop-size distributions in emulsions stabilized with Tween 20 were bimodal. In the case of 0.016 wt% and 0.16 wt% Tween 20, the emulsions were instable after 1 h at 60 °C because of oil drop coalescence (release of oil lenses). The emulsions with 0.5 wt% Tween 20 were stable against coalescence. After 72 h at 60 °C, the drop size distributions of the xylene-in-water emulsions with 0.5 wt% Tween 20 exhibit indications for Ostwald ripening (Fig. 14). In other words, Tween 20 cannot block the Ostwald ripening in xylene-in-water emulsions subjected to heating at 60 °C even at the highest studied concentration of 0.5 wt%.

9. Conclusions

The present paper is the first detailed and systematic study on the properties of hydrophobin HFBII as emulsifier, including both emulsification and emulsion stability. The main results and conclusions are as follows.

The dynamics of interfacial tension relaxation was measured by means of two different techniques, DSA and CPT. The results indicate that below a certain threshold value of the interfacial tension, σ^*, the hydrophobin adsorption layer solidifies not only at the air/water interface [7,11,70], but also at the oil/water interface. Interpretation is given of the different values of σ^* for air/water and oil/water interfaces (Section 4).

The behavior of o/w/o emulsion films was investigated as a model for the interaction between emulsion drops. For the first time, we established that formation of self-assembled bilayer (S-bilayer; final stage of film thinning) is observed not only with foam films [9,20,25], but also with emulsion films. The strong adhesion of the hydrophilic parts of the HFBII molecules in the S-bilayer seems to be insensitive to the nature of the hydrophobic phase: air or oil. At the higher protein concentrations, HFBII aggregates are sandwiched in the emulsion films and block their further thinning, which has a stabilizing effect.

SBO-in-water emulsions have been produced at different HFBII concentrations. The drop size distributions in the emulsions have been determined from video frames taken by optical microscopy. The concentration dependence of the mean drop radius, R_{10}, indicates that at the higher protein concentrations and lower oil volume fractions the emulsification happens in the *Kolmogorov regime* [60–65], i.e. the drop size is determined by the power of homogenizer. In contrast, at the lower protein concentrations and higher oil volume fractions the emulsification happens in the *limited-coalescence* regime [57–59], i.e. the drops undergo several coalescence cycles before reaching a sufficiently high protein surface coverage that blocks the further coalescence (Fig. 8). The growth of bigger protein aggregates with the rise of protein concentration also affects the process of limited coalescence; see Fig. 9 and Eq. (15).

Upon storage, at HFBII concentrations higher than 0.05 wt% the produced SBO-in-water emulsions were very stable, at least for 50 days, without any indications for drop coalescence. From this viewpoint, the previous report that HFBII stabilized emulsions are completely destroyed within 24 h [35] is probably due to the low (ca. 0.01 wt%) protein concentration used.

The emulsions with HFBII are unstable upon stirring. This fact indicates that the solidified hydrophobin adsorption layers on the drop surfaces are fragile and can break under the action of shear stresses. The wrapping of the hydrophobin-covered drops with a second adsorption layer of BLG removes the instability upon stirring (Section 7.2). The layer of BLG can prevent the drop–drop adhesion and can serve as a source of protein molecules that can fill the cracks and voids in the solidified HFBII adsorption layer that appear when the emulsion drops are deformed under the action of shear stresses. The mixing of BLG and HFBII produces also a synergistic effect with respect to the emulsion stability upon centrifugation (Fig. 10a). However, the addition of BLG worsens the emulsion stability upon long storage (Fig. 10b).

Finally, we checked the emulsion stability against Ostwald ripening in the case of volatile oils (limonene and xylene) that exhibit pronounced solubility in the aqueous phase. At concentrations greater than 0.1 wt% (and Φ_{oil} = 30%), HFBII completely blocks the Ostwald ripening in the limonene-in-water emulsions (Fig. 11). In comparative experiments, the worst stability was observed for the emulsions with SMP, in which well pronounced Ostwald ripening was observed (Fig. 12). BLG and Tween 20 could also block the Ostwald ripening at sufficiently high concentrations. In this respect, HFBII has the advantage that it not only suppresses the exchange of oil molecules between the drops (that causes the Ostwald ripening), but also forms *solidified* capsules which can be used for retention of soluble and/or volatile compounds (e.g. fragrances, flavors, colors and preservatives) in the aqueous phase [43]. The HFBII adsorption layers are impermeable for the transfer of volatile oils even at a higher temperature, 60 °C, as indicated by the experiment with xylene-in-water emulsions (Fig. 13).

We hope that the present study on the properties of HFBII stabilized emulsions will broaden the applications of hydrophobins not only as foam-stabilizers, but also as emulsifiers.

Acknowledgments

The authors gratefully acknowledge the support from Unilever R&D. They thank Dr. Rumyana Stanimirova and Mr. Mihail T. Georgiev for their important contributions to the oscillating drop and interfacial tension measurements, respectively.

Appendix A. Supplementary data

Supplementary data associated with this article can be found, in the online version, at http://dx.doi.org/10.1016/j.colsurfa.2016.09.066.

References

[1] M.B. Linder, Hydrophobins: proteins that self assemble at interfaces, Curr. Opin. Colloid Interface Sci. 14 (2009) 356–363.
[2] M. Lienemann, J.-A. Gandier, J.J. Joensuu, A. Iwanaga, Y. Takatsuji, T. Haruyama, E. Master, M. Tenkanen, M.B. Linder, Structure-function relationships in hydrophobins: probing the role of charged side chains, Appl. Environ. Microbiol. 79 (2013) 5533–5538.
[3] H.A.B. Wösten, K. Scholtmeijer, Applications of hydrophobins: current state and perspectives, Appl. Microbiol. Biotechnol. 99 (2015) 1587–1597.
[4] I.M. Tucker, J.T. Petkov, J. Penfold, R.K. Thomas, A.R. Cox, N. Hedges, Adsorption of hydrophobin-protein mixtures at the air-water interface: the impact of pH and electrolyte, Langmuir 31 (2015) 10008–10016.
[5] T.B.J. Blijdenstein, P.W.N. de Groot, S.D. Stoyanov, On the link between foam coarsening and surface rheology: why hydrophobins are so different, Soft Matter 6 (2010) 1799–1808.
[6] K.D. Danov, G.M. Radulova, P.A. Kralchevsky, K. Golemanov, S.D. Stoyanov, Surface shear rheology of hydrophobin adsorption layers: laws of viscoelastic behaviour with applications to long-term foam stability, Faraday Discuss. 158 (2012) 195–221.
[7] N.A. Alexandrov, K.G. Marinova, T.D. Gurkov, K.D. Danov, P.A. Kralchevsky, S.D. Stoyanov, T.B.J. Blijdenstein, L.N. Arnaudov, E.G. Pelan, A. Lips, Interfacial layers from the protein HFBII hydrophobin: dynamic surface tension, dilatational elasticity and relaxation times, J. Colloid Interface Sci. 376 (2012) 296–306.
[8] E. Aumaitre, S. Wongsuwarn, D. Rossetti, N.D. Hedges, A.R. Cox, D. Vella, P. Cicuta, A viscoelastic regime in dilute hydrophobin monolayers, Soft Matter 8 (2012) 1175–1183.
[9] K.D. Danov, P.A. Kralchevsky, G.M. Radulova, E.S. Basheva, S.D. Stoyanov, E.G. Pelan, Shear rheology of mixed protein adsorption layers vs their structure studied by surface force measurements, Adv. Colloid Interface Sci. 222 (2015) 148–161.

[10] S. Knoche, D. Vella, E. Aumaitre, P. Degen, H. Rehage, P. Cicuta, J. Kierfeld, Elastometry of deflated capsules: elastic moduli from shape and wrinkle analysis, Langmuir 29 (2013) 12463–12471.
[11] K.D. Danov, R.D. Stanimirova, P.A. Kralchevsky, K.G. Marinova, S.D. Stoyanov, T.B.J. Blijdenstein, A.R. Cox, E.G. Pelan, Adhesion of bubbles and drops to solid surfaces, and anisotropic surface tensions studied by capillary meniscus dynamometry, Adv. Colloid Interface Sci. 233 (2016) 223–239.
[12] M. Qin, L.-K. Wang, X.-Z. Feng, Y.-L. Yang, R. Wang, C. Wang, L. Yu, B. Shao, M.-Q. Qiao, Bioactive surface modification of mica and poly(dimethylsiloxane) with hydrophobins for protein immobilization, Langmuir 23 (2007) 4465–4471.
[13] X. Li, S. Hou, X. Feng, Y. Yu, J. Ma, L. Li, Patterning of neural stem cells on poly(lactic-*co*-glycolic acid) film modified by hydrophobin, Colloids Surf. B 74 (2009) 370–374.
[14] J. Hakanpää, A. Paananen, A. Askolin, T. Nakari-Setälä, T. Parkkinen, M. Penttilä, M.B. Linder, J. Rouvinen, Atomic resolution structure of the HFBII hydrophobin, a self-assembling amphiphile, J. Biol. Chem. 279 (2004) 534–539.
[15] M. Torkkeli, R. Serimaa, O. Ikkala, M. Linder, Aggregation and self-assembly of hydrophobins from *Trichoderma reesei*: low-resolution structural model, Biophys. J. 83 (2002) 2240–2247.
[16] G.R. Szilvay, T. Nakari-Setälä, M.B. Linder, Behavior of *Trichoderma reesei* hydrophobins in solution: interactions, dynamics, and multimer formation, Biochemistry 45 (2006) 8590–8598.
[17] K. Kisko, G.R. Szilvay, U. Vainio, M.B. Linder, Interactions of hydrophobin proteins in solution studied by small-angle X-ray scattering, Biophys. J. 94 (2008) 198–206.
[18] K. Kisko, G.R. Szilvay, E. Vuorimaa, H. Lemmetyinen, M.B. Linder, M. Torkkeli, R. Serimaa, Self-assembled films of hydrophobin proteins HFBI and HFBII studied in situ at the air/water interface, Langmuir 25 (2009) 1612–1619.
[19] A.R. Cox, F. Cagnol, A.B. Russell, M.J. Izzard, Surface properties of class II hydrophobins from Trichoderma reesei and influence on bubble stability, Langmuir 23 (2007) 7995–8002.
[20] E.S. Basheva, P.A. Kralchevsky, N.C. Christov, K.D. Danov, S.D. Stoyanov, T.B.J. Blijdenstein, H.-J. Kim, E.G. Pelan, A. Lips, Unique properties of bubbles and foam films stabilized by HFBII hydrophobin, Langmuir 27 (2011) 2382–2392.
[21] X.L. Zhang, J. Penfold, R.K. Thomas, I.M. Tucker, J.T. Petkov, J. Bent, A. Cox, I. Grillo, Self-assembly of hydrophobin and hydrophobin/surfactant mixtures in aqueous solution, Langmuir 27 (2011) 10514–10522.
[22] X.L. Zhang, J. Penfold, R.K. Thomas, I.M. Tucker, J.T. Petkov, J. Bent, A. Cox, R.A. Campbell, Adsorption behavior of hydrophobin and hydrophobin/surfactant mixtures at the air–water interface, Langmuir 27 (2011) 11316–11323.
[23] X.L. Zhang, J. Penfold, R.K. Thomas, I.M. Tucker, J.T. Petkov, J. Bent, A. Cox, Adsorption behavior of hydrophobin and hydrophobin/surfactant mixtures at the solid–solution interface, Langmuir 27 (2011) 10464–10474.
[24] I.M. Tucker, J.T. Petkov, J. Penfold, R.K. Thomas, A.R. Cox, N. Hedges, Adsorption of hydrophobin/β-casein mixtures at the solid-liquid interface, J. Colloid Interface Sci. 478 (2016) 81–87.
[25] E.S. Basheva, P.A. Kralchevsky, K.D. Danov, S.D. Stoyanov, T.B.J. Blijdenstein, E.G. Pelan, A. Lips, Self-assembled bilayers from the protein HFBII hydrophobin: nature of the adhesion energy, Langmuir 27 (2011) 4481–4488.
[26] A.R. Cox, D.L. Aldred, A.B. Russell, Exceptional stability of food foams using class II hydrophobin HFBII, Food Hydrocoll. 23 (2009) 366–376.
[27] T.B.J. Blijdenstein, R.A. Ganzevles, P.W.N. de Groot, S.D. Stoyanov, On the link between surface rheology and foam disproportionation in mixed hydrophobin HFBII and whey protein systems, Colloids Surf. A 438 (2013) 13–20.
[28] E. Dickinson, Exploring the frontiers of colloidal behaviour where polymers and particles meet, Food Hydrocoll. 52 (2016) 497–509.
[29] S. Tcholakova, Z. Mitrinova, K. Golemanov, N.D. Denkov, M. Vethamuthu, K.P. Ananthapadmanabhan, Control of Ostwald ripening by using surfactants with high surface modulus, Langmuir 27 (2011) 14807–14819.
[30] L.M. Dimitrova, P.V. Petkov, P.A. Kralchevsky, S.D. Stoyanov, E.G. Pelan, Production and characterization of stable foams with fine bubbles from solutions of hydrophobin HFBII and its mixtures with other proteins, Colloids Surf. A (2016), http://dx.doi.org/10.1016/j.colsurfa.2016.06.018.
[31] H.A.B. Wösten, F.H.J. Schuren, J.G.H. Wessels, Interfacial self-assembly of a hydrophobin into an amphipathic membrane mediates fungal attachment to hydrophobic surfaces, EMBO J. 13 (1994) 5848–5854.
[32] J.G.H. Wessels, Hydrophobins: proteins that change the nature of the fungal surface, Adv. Microb. Physiol. 38 (1997) 1–45.
[33] K. Scholtmeijer, J.G.H. Wessels, H.A.B. Wösten, Fungal hydrophobins in medical and technical applications, Appl. Microbiol. Biotechnol. 56 (2001) 1–8.
[34] S.O. Lumsdon, J. Green, B. Stieglitz, Adsorption of hydrophobin proteins at hydrophobic and hydrophilic interfaces, Colloids Surf. B 44 (2005) 172–178.
[35] S. Askolin, M. Linder, K. Scholtmeijer, M. Tenkanen, M. Penttilä, M.L. de Vocht, H.A.B. Wösten, Interaction and comparison of a class I hydrophobin from *Schizophyllum commune* and class II hydrophobins from *Trichoderma reesei*, Biomacromolecules 7 (2006) 1295–1301.
[36] M. Reger, T. Sekine, T. Okamoto, H. Hoffmann, Unique emulsions based on biotechnically produced hydrophobins, Soft Matter 7 (2011) 8248–8257.
[37] M. Reger, T. Sekine, T. Okamoto, K. Watanabe, H. Hoffmann, Pickering emulsions stabilized by novel clay?hydrophobin synergism, Soft Matter 7 (2011) 11021–11030.
[38] M. Reger, H. Hoffmann, Hydrophobin coated boehmite nanoparticles stabilizing oil in water emulsions, J. Colloid Interface Sci. 368 (2012) 378–386.
[39] M. Reger, T. Sekine, H. Hoffmann, Boosting the stability of protein emulsions by the synergistic use of proteins and clays, Colloid Polym. Sci. 290 (2012) 631–640.
[40] H. Hoffmann, M. Reger, Emulsions with unique properties from proteins as emulsifiers, Adv. Colloid Interface Sci. 205 (2014) 94–104.
[41] F.L. Tchuenbou-Magaia, I.T. Norton, P.W. Cox, Hydrophobins stabilised air-filled emulsions for the food industry, Food Hydrocoll. 23 (2009) 1877–1885.
[42] A.J. Green, K.A. Littlejohn, P. Hooley, P.W. Cox, Formation and stability of food foams and aerated emulsions: hydrophobins as novel functional ingredients, Curr. Opin. Colloid Interface Sci. 18 (2013) 292–301.
[43] M. Khalesi, N. Mandelings, B. Herrera-Malaver, D. Riveros-Galan, K. Gebruers, G. Derdelinckx, Improvement of the retention of ocimene in water phase using Class II hydrophobin HFBII, Flavour Fragr. J. 30 (2015) 451–458.
[44] A. Schulz, M. Fioroni, M.B. Linder, A. Nessel, M. Bocola, T. Subkowski, U. Schwaneberg, A. Böker, F. Rodríguez-Ropero, Exploring the mineralization of hydrophobins at a liquid interface, Soft Matter 8 (2012) 11343–11352.
[45] G.M. Radulova, K.D. Danov, P.A. Kralchevsky, J.T. Petkov, S.D. Stoyanov, Shear rheology of hydrophobin adsorption layers at oil/water interfaces and data interpretation in terms of a viscoelastic thixotropic model, Soft Matter 10 (2014) 5777–5786.
[46] D. Georgieva, V. Schmitt, F. Leal-Calderon, D. Langevin, On the possible role of surface elasticity in emulsion stability, Langmuir 25 (2009) 5565–5573.
[47] J. Krägel, R. Wüstneck, F. Husband, P.J. Wilde, A.V. Makievski, D.O. Grigoriev, J.B. Li, Properties of mixed protein/surfactant adsorption layers, Colloids Surf. B 12 (1999) 399–407.
[48] A.G. Gaonkar, R.P. Borwankar, Adsorption behavior of monoglycerides at the vegetable oil/water interface, J. Colloid Interface Sci. 146 (1991) 525–532.
[49] J. Santos, G.T. Vladisavljević, R.G. Holdich, M.M. Dragosavac, J. Muñoz, Controlled production of eco-friendly emulsions using direct and premix membrane emulsification, Chem. Eng. Res. Des. 98 (2015) 59–69.
[50] S.H. Yalkowsky, Y. He, P. Jain, Handbook of Aqueous Solubility Data, CRC Press, Boca Raton, FL, 2010.
[51] S.C. Russev, N. Alexandrov, K.G. Marinova, K.D. Danov, N.D. Denkov, L. Lyutov, V. Vulchev, C. Bilke-Krause, Instrument and methods for surface dilatational rheology measurements, Rev. Sci. Instrum. 79 (2008) 104102.
[52] A. Sheludko, Thin liquid films, Adv. Colloid Interface Sci. 1 (1967) 391–464.
[53] K.G. Marinova, T.D. Gurkov, O.D. Velev, I.B. Ivanov, B. Campbell, R.P. Borwankar, The role of additives for the behaviour of thin emulsion films stabilized by proteins, Colloids Surf. A 123–124 (1997) 155–167.
[54] N.C. Christov, K.D. Danov, D.K. Danova, P.A. Kralchevsky, The drop size in membrane emulsification determined from the balance of capillary and hydrodynamic forces, Langmuir 24 (2008) 1397–1410.
[55] G.A. Korn, T.M. Korn, Mathematical Handbook, McGraw-Hill, New York, 1968.
[56] R.M. Wiley, Limited coalescence of oil droplets in coarse oil-in-water emulsions, J. Colloid Sci. 9 (1954) 427–437.
[57] T.H. Whitesides, D.S. Ross, Experimental and theoretical analysis of the limited coalescence process: stepwise limited coalescence, J. Colloid Interface Sci. 169 (1995) 48–59.
[58] S. Arditty, C.P. Whitby, B.P. Binks, V. Schmitt, F. Leal-Calderon, Some general features of limited coalescence in solid-stabilized emulsions, Eur. Phys. J. E 11 (2003) 273–281.
[59] K. Golemanov, S. Tcholakova, P.A. Kralchevsky, K.P. Ananthapadmanabhan, A. Lips, Latex-particle-stabilized emulsions of anti-Bancroft type, Langmuir 22 (2006) 4968–4977.
[60] A.N. Kolmogorov, On the breakage of drops in a turbulent flow, Dokl. Akad. Nauk SSSR 66 (1949) 825–828 (in Russian).
[61] J.O. Hinze, Fundamentals of the hydrodynamic mechanism of splitting in dispersion processes, AIChE J. 3 (1955) 289–295.
[62] P. Walstra, Formation of emulsions, in: P. Becher (Ed.), Encyclopedia of Emulsion Technology, vol. 1, Marcel Dekker, New York, 1983, pp. 57–127, Chapter 2.
[63] P. Walstra, T.J. Geurts, A. Noomen, A. Jellema, M.A.J. van Boekel, Dairy Technology, Marcel Dekker, New York, 1999.
[64] S. Tcholakova, N.D. Denkov, T. Danner, Role of surfactant type and concentration for the mean drop size during emulsification in turbulent flow, Langmuir 20 (2004) 7444–7458.
[65] S. Tcholakova, N.D. Denkov, I.B. Ivanov, B. Campbell, Coalescence stability of emulsions containing globular milk proteins, Adv. Colloid Interface Sci. 123–126 (2006) 259–293.
[66] H. Jin, W. Zhou, J. Cao, S.D. Stoyanov, T.B.J. Blijdenstein, P.W.N. de Groot, L.N. Arnaudov, E.G. Pelan, Super stable foams stabilized by colloidal ethyl cellulose particles, Soft Matter 8 (2012) 2194–2205.
[67] S. Tcholakova, N.D. Denkov, I.B. Ivanov, B. Campbell, Coalescence in β-lactoglobulin-stabilized emulsions: effects of protein adsorption and drop size, Langmuir 18 (2002) 8960–8971.
[68] S. Tcholakova, N.D. Denkov, D. Sidzhakova, I.B. Ivanov, B. Campbell, Interrelation between drop size and protein adsorption at various emulsification conditions, Langmuir 19 (2003) 5640–5649.
[69] H. Fisher, I. Polikarpov, A.F. Craievich, Average protein density is a molecular-weight-dependent function, Protein Sci. 13 (2004) 2825–2828.
[70] K.D. Danov, R.D. Stanimirova, P.A. Kralchevsky, K.G. Marinova, N.A. Alexandrov, S.D. Stoyanov, T.B.J. Blijdenstein, E.G. Pelan, Capillary meniscus dynamometry-method for determining the surface tension of drops and bubbles with isotropic and anisotropic surface stress distributions, J. Colloid Interface Sci. 440 (2015) 168–178.

[71] R.D. Stanimirova, K.G. Marinova, K.D. Danov, P.A. Kralchevsky, E.S. Basheva, S.D. Stoyanov, E.G. Pelan, Competitive adsorption of the protein hydrophobin and an ionic surfactant: parallel vs sequential adsorption and dilatational rheology, Colloids Surf. A 457 (2014) 307–317.
[72] M. Schmitt-Rozières, J. Krägel, D.O. Grigoriev, L. Liggieri, R. Miller, S. Vincent-Bonnieu, M. Antoni, From spherical to polymorphous dispersed phase transition in water/oil emulsions, Langmuir 25 (2009) 4266–4270.
[73] J. Squier, M. Müller, High resolution nonlinear microscopy: a review of sources and methods for achieving optimal imaging, Rev. Sci. Instrum. 72 (2001) 2855–2867.
[74] I. Popa, G. Gillies, G. Papastavrou, M. Borkovec, Attractive electrostatic forces between identical colloidal particles induced by adsorbed polyelectrolytes, J. Phys. Chem. B 113 (2009) 8458–8461.
[75] P.R. Majhi, R.R. Ganta, R.P. Vanam, E. Seyrek, K. Giger, P.L. Dubin, Electrostatically driven protein aggregation: β-lactoglobulin at low ionic strength, Langmuir 22 (2006) 9150–9159.

Appendix A. Supplementary Data

for the article

Limited coalescence and Ostwald ripening in emulsions stabilized by hydrophobin HFBII and milk proteins

Lydia M. Dimitrova [a], Mariana P. Boneva [a], Krassimir D. Danov [a], Peter A. Kralchevsky [a,*], Elka S. Basheva [a], Krastanka G. Marinova [a], Jordan T. Petkov [b], Simeon D. Stoyanov [c,d,e]

[a] *Department of Chemical and Pharmaceutical Engineering, Faculty of Chemistry and Pharmacy, Sofia University, 1164 Sofia, Bulgaria*

[b] *Unilever Research & Development, Port Sunlight, Wirral, Merseyside CH63 3JW, U.K.*

[c] *Unilever Research & Development Vlaardingen, 3133AT Vlaardingen, The Netherlands*

[d] *Laboratory of Physical Chemistry and Colloid Science, Wageningen University, 6703 HB Wageningen, The Netherlands*

[e] *Department of Mechanical Engineering, University College London, WC1E 7JE, UK*

Here, the reference numbers are the same as in the main text of the article.

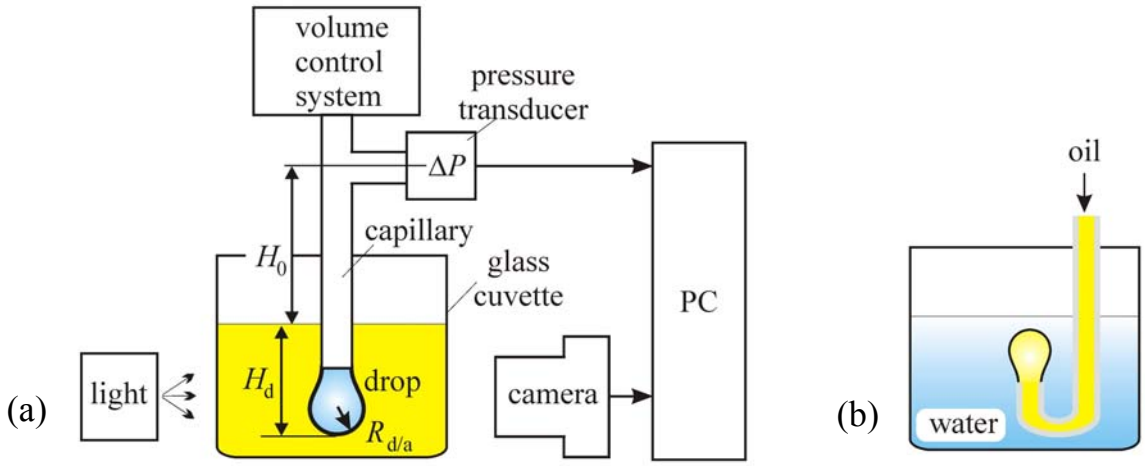

Fig. A.1. (a) Sketch of the used DSA100M system for DSA and CPT measurements of interfacial tension. In the case of CPT, the capillary pressure was measured by a pressure transducer, whereas in the case of DSA, only the drop profile was processed [47]. (b) Sketch of a J-shaped capillary used in the measurements with buoyant oil drops. For the studied protein concentrations, the measurements with pendant water drops in oil and buoyant oil drops in water gave the same results, i.e. there are no solution exhaustion effects due to the small size of the drop.

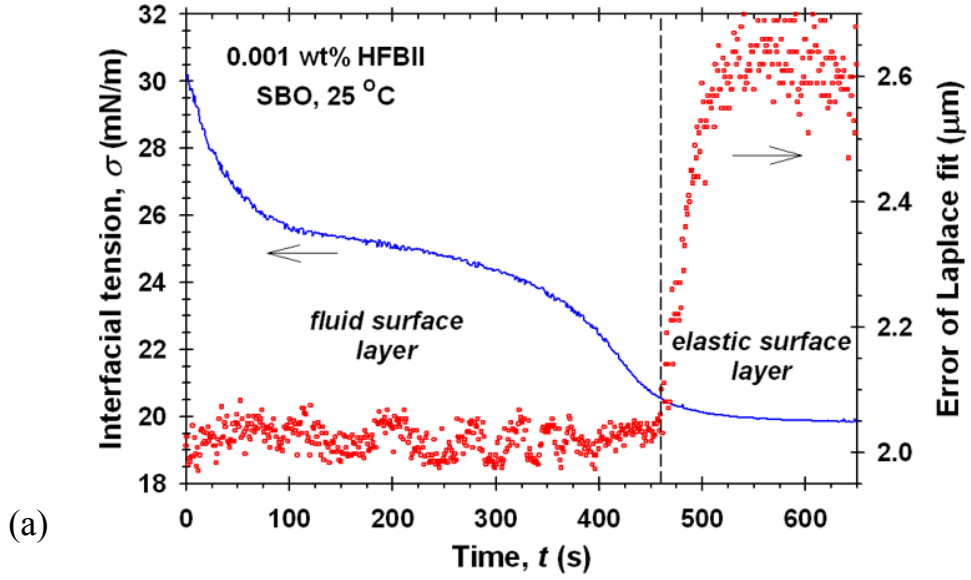

(a)

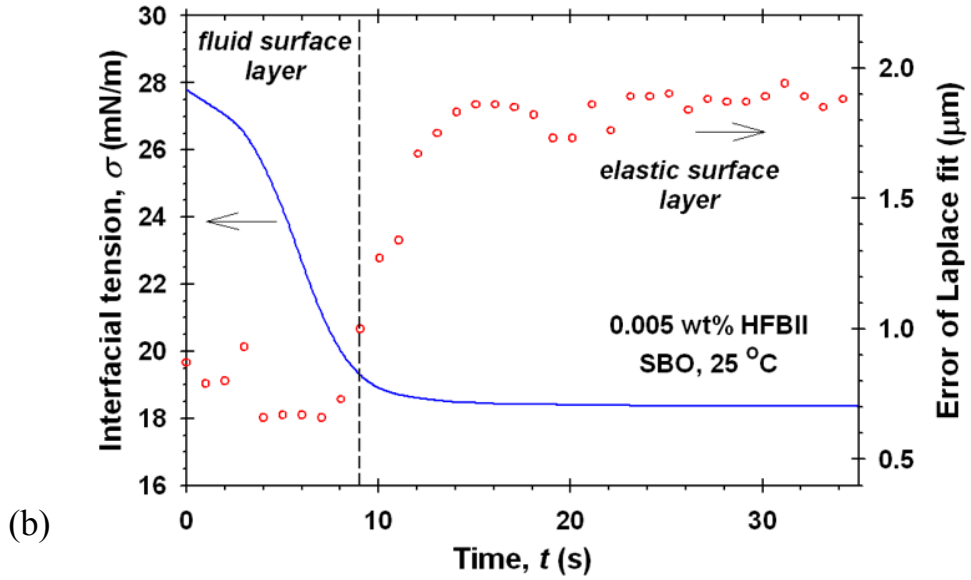

(b)

Fig. A.2. Time dependencies of the interfacial tension and of the error of the fit of the drop profile by means of the Laplace differential equation of capillarity: pendant drop method + DSA at (a) 0.001 wt% HFBII in the water phase; (b) 0.005 wt% HFBII in the water phase; the oil phase is SBO. The increase of the fit error for $\sigma > 21$ mN/m indicates deviation from the Laplace shape due to solidification of the protein adsorption layer.

(a) (b) (c)

Fig. A.3. HFBII-stabilized emulsion films with fresh oil/water interfaces: (a–c) evolution of a o/w/o film from aqueous solution with 10^{-3} wt % HFBII – fast transition to S-bilayer, which is stable. Photos for aged interfaces are not shown, because there was no difference with fresh interfaces. The horizontal length of each photo corresponds to 300 μm.

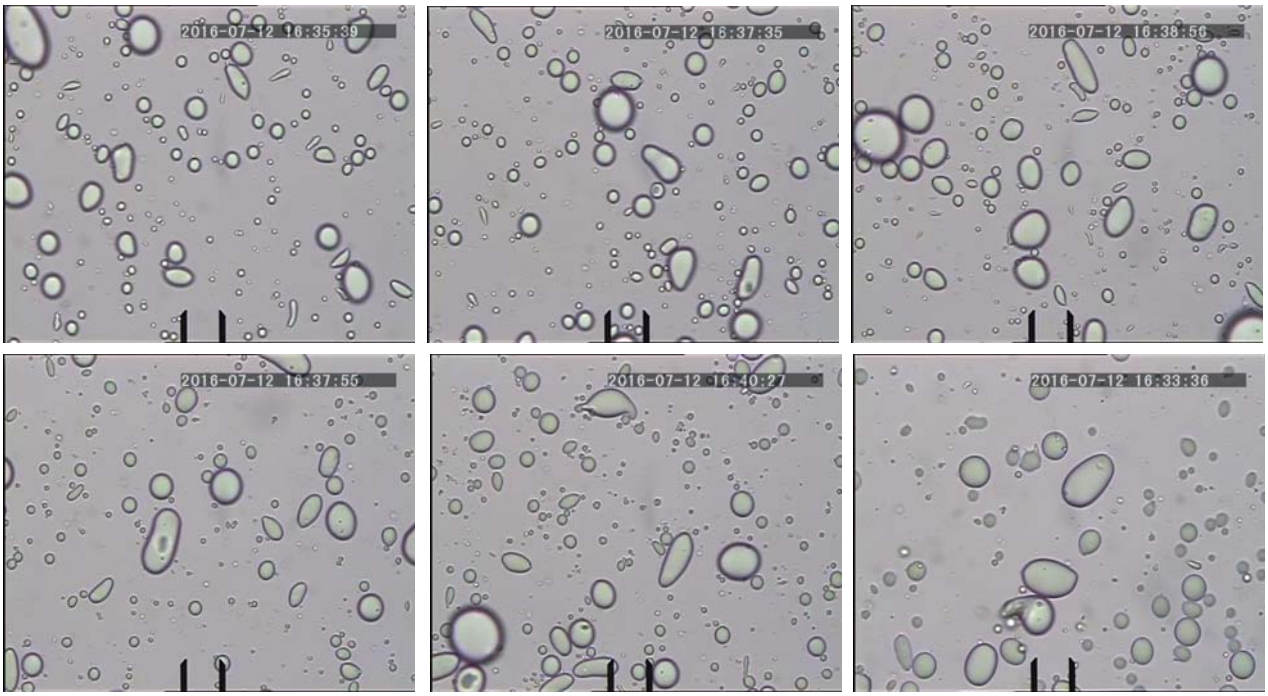

Fig. A.4. Video frames with images of a diluted emulsion SBO-in-water prepared with 30% initial oil volume fraction and 2:1 BLG/HFBII in the aqueous phase at total initial protein concentration 0.25 wt%. After the dilution with water and gentle stirring, the emulsion remains stable and the droplets preserve their, in general, non-spherical shapes. These results are consistent with a model of bilayer protein coverage of the oil drops [9]. The first layer is from HFBII, which is solidified and supports the non-spherical shapes. The second layer is of BLG. Its role is to prevent the drop coalescence when the emulsion is subjected to the action of shear stresses upon stirring (see Section 7.2). The reference mark is 20 μm.

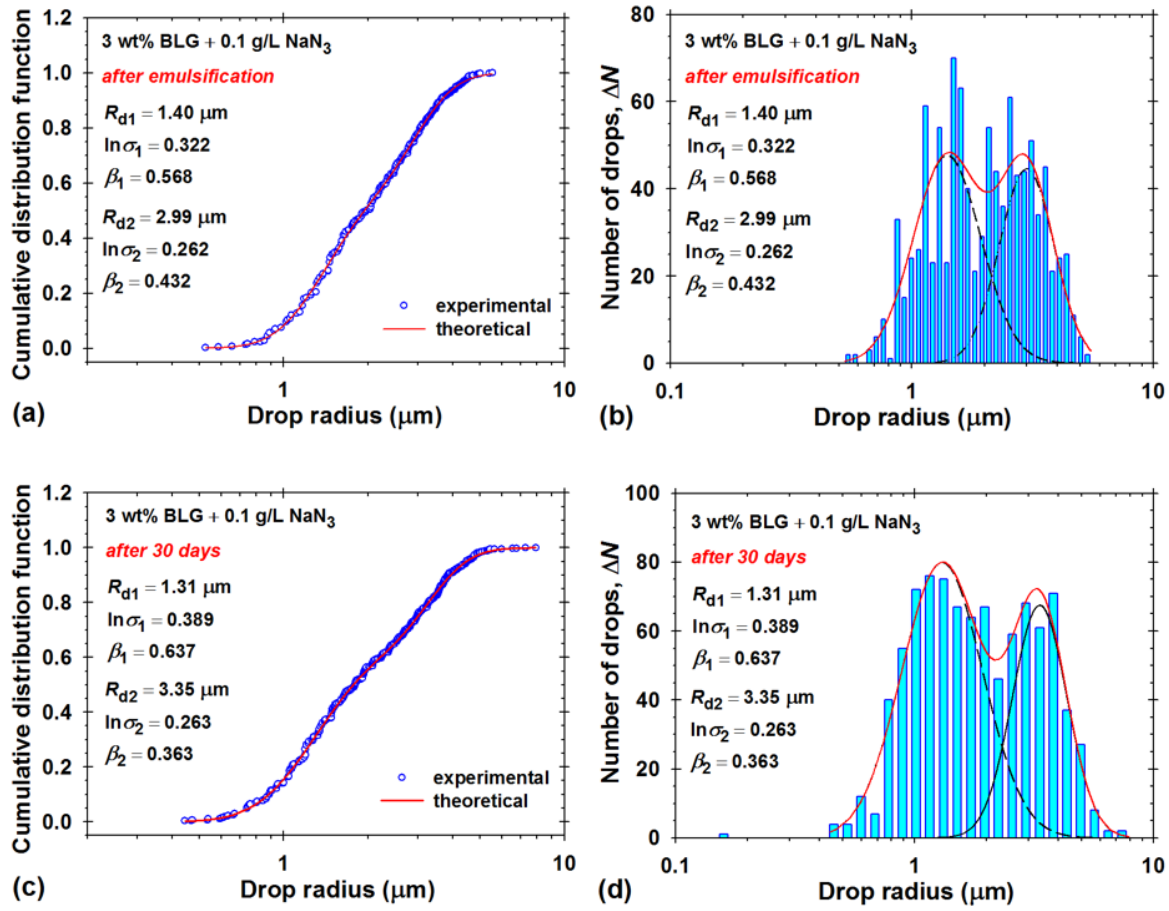

Fig. A.5. Data for limonene-in-water emulsions (Φ_{oil} = 0.30) stabilized with 3 wt% BLG in the water phase. (a,c) Plots of the cumulative function vs. the drop radius and (b,d) drop-size distributions. The solid line represents the best fit with a bimodal lognormal distribution for the data after 0 and 30 days of storage at 25 ºC. The dashed lines show the two constituent unimodal distributions. There are weak indications for Ostwald ripening.

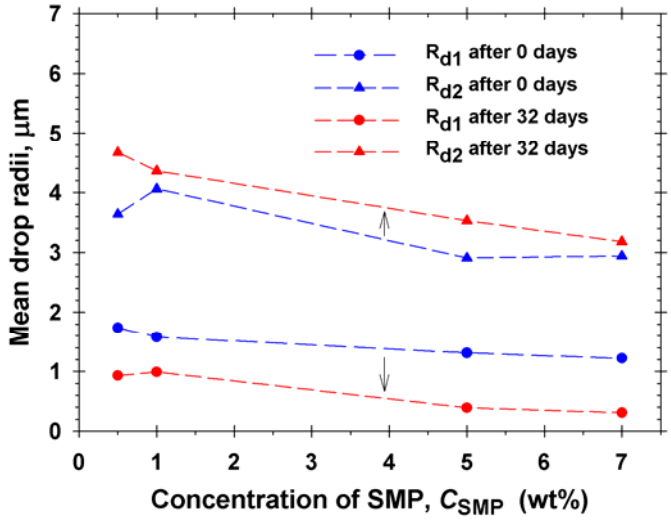

Fig. A.6. Data for limonene-in-water emulsions (Φ_{oil} = 0.30) stabilized with 5 wt % SMP in the water phase. Comparison of the mean drop radii R_{d1} and R_{d2} determined from the best fit of the respective cumulative functions for the same emulsion after storage for 0 and 32 days. The data indicate that the size of the smaller drops decreases, whereas the size of the larger drops increases with time, which is typical for Ostwald ripening.

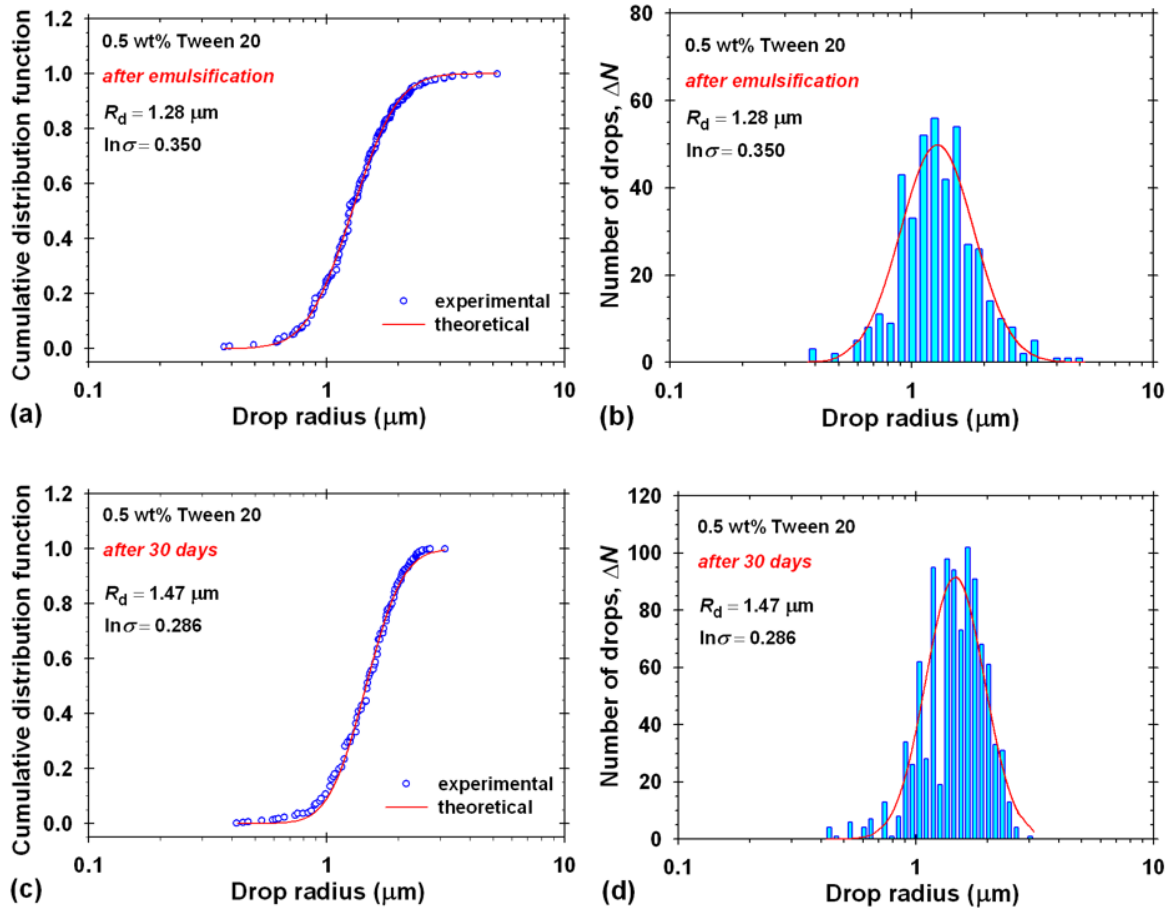

Fig. A.7. Data for limonene-in-water emulsions (Φ_{oil} = 0.30) stabilized with 0.5 wt% BLG in the water phase. (a,c) Plots of the cumulative function vs. the drop radius and (b,d) drop-size distributions. The solid line represents the best fit with a bimodal lognormal distribution for the data after 0 and 30 days of storage at 25 ºC. The dashed lines show the two constituent unimodal distributions. There are no indications for Ostwald ripening.

Table A1. Values of the mean drop radius, R_{10}, and its standard error for different hydrophobin concentrations, C_{HFBII}, corresponding to the experimental points in Fig. 8 of the main text.

10 vol% SBO			30 vol% SBO			50 vol% SBO		
C_{HFBII} (wt%)	R_{10} (μm)	Std.err.	C_{HFBII} (wt%)	R_{10} (μm)	Std.err.	C_{HFBII} (wt%)	R_{10} (μm)	Std.err.
0.05	1.60	0.03	0.05	7.84	0.10	0.05	7.91	0.17
0.1	1.19	0.05	0.1	4.29	0.06	0.1	3.81	0.11
0.25	1.05	0.02	0.25	1.37	0.04	0.5	1.52	0.04
0.5	1.62	0.04	0.5	2.22	0.03	1	0.94	0.03
1	0.93	0.03	1	1.7	0.04	5	1.71	0.04
1.5	1.99	0.04	1.5	1.37	0.02	–	–	–
3	1.06	0.04	3	1.34	0.03	–	–	–
5	1.27	0.04	4.67	1.99	0.04	–	–	–
7	1.66	0.06	7	1.47	0.04	–	–	–

Table A2. Values of the mean drop radius, R_{10}, and its standard error for different protein concentrations corresponding to the experimental points in Fig. 10b of the main text.

(A) BLG

0 days storage			50 days storage		
C_{BLG} (wt%)	R_{10} (μm)	Std.err.	C_{BLG} (wt%)	R_{10} (μm)	Std.err.
0.05	3.38	0.13			
0.1	2.79	0.10	0.1	7.11	0.18
0.25	1.09	0.04	0.25	4.94	0.11
0.5	1.13	0.04	0.5	2.84	0.05
1	1.72	0.06	1	2.79	0.04
1.5	1.51	0.06	1.5	2.18	0.04
3	1.37	0.06	3	2.29	0.05
5	1.61	0.06	5	2.69	0.05

(B) 2:1 BLG:HFBII

0 days storage			50 days storage		
$C_{BLG:HFBII\ (2:1)}$ (wt%)	R_{10} (μm)	Std.err.	$C_{BLG:HFBII\ (2:1)}$ (wt%)	R_{10} (μm)	Std.err.
0.05	4.68	0.18	0.05	9.62	0.28
0.1	2.14	0.10	0.1	7.64	0.15
0.25	1.55	0.06	0.25	3.55	0.07
0.5	1.01	0.04	0.5	3.27	0.06
1	1.59	0.05	1	2.47	0.06
3	1.36	0.04	3	2.46	0.04